Thesis for The Degree of Doctor of Philosophy

Modeling cloud phase in the Arctic and globally

Hannah C. Frostenberg

Department of Environmental and Energy Sciences
Chalmers University of Technology
Göteborg, Sweden, 2026

Modeling cloud phase in the Arctic and globally
Hannah C. Frostenberg
ISBN 978-91-8103-416-5

Acknowledgements, dedications, and similar personal statements in this thesis, reflect the author's own views.

© Hannah C. Frostenberg, 2026
except where otherwise stated.
All rights reserved.

Doktorsavhandlingar vid Chalmers tekniska högskola
Ny serie nr 5873
ISSN 0346-718X
DOI 10.63959/chalmers.dt/5873

Department of Environmental and Energy Sciences
Division of Geoscience and Remote Sensing
Chalmers University of Technology
SE-412 96 Göteborg,
Sweden
Phone: +46 (0) 31 772 1000

Cover: Mixed-phase clouds over Arctic sea ice during ARTofMELT.
© Luisa Ickes

Printed by Chalmers Digitaltryck,
Göteborg, Sweden 2026.

Modeling cloud phase in the Arctic and globally

Hannah C. Frostenberg

Department of Environmental and Energy Sciences
Chalmers University of Technology

Abstract

The phase of cloud hydrometeors critically modulates the impact of clouds on the global energy balance. In the Arctic, this phase partitioning influences the timing of sea ice melt and freeze. Mixed-phase clouds (MPCs) consist of both liquid and ice phases, requiring models to accurately simulate this apportionment to represent the climate system. Yet, MPCs remain difficult to simulate. This thesis advances the modeling of microphysical processes that govern phase evolution in MPCs through a multi-scale approach using large-eddy simulations (LES) and general circulation models (GCMs).

The research introduces a stochastic ice nucleation parameterization to address the limitations of existing schemes. Applying this method to LES of an Arctic MPC produced ice mass magnitudes consistent with observations. However, the scheme was sensitive to model resolution; resolving this dependency is a prerequisite for its application to improve ice representation across both LES and GCM scales. Extending the investigation of ice nucleation, a sensitivity analysis across three GCMs revealed diverging relative importance of four microphysical processes, including ice nucleation. Even a unified secondary ice production parameterization caused varying model responses, ranging from negligible changes to substantial global impacts. The lack of consensus further illustrates the challenges of modeling cloud microphysics and questions the traditional representation of microphysics as a chain of individual processes. A sensitivity analysis of a separate Arctic MPC showed that the concentrations of droplet-forming aerosol particles and ice crystals dominated the liquid and ice mass, respectively. Ice crystal shape proved less influential for the absolute magnitudes of these phases, yet it dictated whether the cloud remained mixed-phase, glaciated, or evolved into a purely liquid cloud. These findings emphasize that models must explicitly account for ice crystal shape and that observational campaigns should prioritize measuring both concentrations and shape at cloud level rather than the surface.

Overall, this thesis advances the representation and understanding of microphysics by providing a new ice nucleation parameterization, challenging the current global modeling approach of sequencing microphysical processes, and highlighting the critical role of ice crystal shape for the cloud phase.

Keywords

Mixed-phase clouds, cloud microphysics, large-eddy simulation, general circulation models, Arctic.

List of publications

Appended publications

This thesis is based on the following appended papers:

Paper 1. Hannah C. Frostenberg, André Welti, Mikael Luhr, Julien Savre, Erik S. Thomson, Luisa Ickes (2023), *The chance of freezing – a conceptional study to parameterize temperature-dependent freezing by including randomness of ice-nucleating particle concentrations.*
Atmospheric Chemistry and Physics. DOI: 10.5194/acp-23-10883-2023

Paper 2. Hannah C. Frostenberg, Montserrat Costa-Surós, Paraskevi Georgakaki, Ulrike Proske, Georgia Sotiropoulou, Eleanor May, David Neubauer, Patrick Eriksson, María Gonçalves Ageitos, Athanasios Nenes, Carlos Pérez García-Pando, Øyvind Seland, Luisa Ickes (2026), *Large discrepancies in dominant microphysical processes governing mixed-phase clouds across climate models.*
NPJ Climate and Atmospheric Science. DOI: 10.1038/s41612-026-01342-7

Paper 3. Hannah C. Frostenberg, Jessie M. Creamean, Erik S. Thomson, Heather Guy, Roman Pohorsky, Camille Mavis, Ian M. Brooks, Nicolas Fauré, Lea Haberstock, Julia Kojoj, Sonia Murto, Julia Schmale, Michael Tjernström, Paul Zieger, Luisa Ickes (2026), *Cloud-phase sensitivities of a simulated Arctic stratocumulus to aerosol and microphysical parameters. Manuscript submitted to Atmospheric Chemistry and Physics.*

Author contributions

Paper 1: I developed the study design in collaboration with Luisa Ickes. I implemented the scheme into the model, and executed all simulations. In close collaboration with Luisa Ickes, I analyzed and visualized the data. I prepared the manuscript under the guidance of Luisa Ickes, incorporating revisions and comments from all coauthors.

Paper 2: I co-led the study with Luisa Ickes, managing the analysis and coordinating the interpretation of results with the coauthor group. I produced the visualizations and developed post-processing scripts for two of the three models. I drafted the manuscript with guidance from Luisa Ickes; two sections were provided by coauthors. Final refinements were based on comments from all coauthors.

Paper 3: I contributed to the discussions that formed the main study goals. I performed the simulations and visualizations and conducted the primary analysis. I prepared the manuscript with supervision from Luisa Ickes and comments from all coauthors.

The large language model Google Gemini was used for the language editing of this thesis. All final content was reviewed and approved by me.

Other relevant publications co-authored by Hannah C. Frostenberg:
Luís Filipe Escusa dos Santos, **Hannah C. Frostenberg**, Alejandro Baró Pérez, Annica M. L. Ekman, Luisa Ickes, and Erik S. Thomson (2025), *Potential impacts of marine fuel regulations on an Arctic stratocumulus case and its radiative response.*
Atmospheric Chemistry and Physics. DOI: 10.5194/acp-25-119-2025

Contents

Acknowledgments

This PhD journey would not have been possible without all the people around me that supported me in many different ways.

I want to give a special thank you to my supervisor Luisa for our many discussions, your guidance, patience, and availability. Your way of supervising with empathy, clear communication, and consistent support made this journey a truly positive experience and I am very grateful that I got to be your PhD student!

Thanks to my assistant supervisor Patrick and additional supervisor Erik at GU for discussions and input over these years, and I particularly appreciate the insights and time Erik offered for our coauthored papers and this thesis.

Jessie and Camille and everybody else in the Kreidenweis-group in Fort Collins: thank you for hosting me for three months and reminding me how much hard work goes into one INP(T) line on a plot!

I also want to thank the MIMICA community, especially Julien in Munich, Nazario, Alejandro, and Annica in Stockholm, as well as Lloyd and Luis in Gothenburg. It is great to have this community for support and to discuss common (or specific) modeling problems!

Thanks to everybody on our corridor for the great work environment, and especially my fellow PhD students for sharing our small and big struggles.

A big thank you goes to my family and friends for support and diversion from PhD life. And the biggest to Tobi, for your incredible support, especially during this final stretch, your steady encouragement, and everything else. Together with Lambda and Anton, you are a great anchor to life outside of work.

Hannah Frostenberg
Göteborg, May 2026

List of abbreviations

AMPS	Arctic Mixed-Phase Stratiform cloud
ARTofMELT	Atmospheric Rivers and the onseT of sea ice MELT
ASCOS	Arctic Summer Cloud Ocean Study
BL	Boundary Layer
CALIOP	Cloud and Aerosol Lidar with Orthogonal Polarization
CALIPSO	Cloud-Aerosol Lidar and Infrared Pathfinder Satellite Observations
CCN	Cloud Condensation Nuclei
CFDC	Continuous Flow Diffusion Chambers
CMIP	Coupled Model Intercomparison Project
CSU	Colorado State University
DWLW	DownWard LongWave radiation at the surface
ESM	Earth System Model
GCM	General Circulation Model
GOCCP	GCM-Oriented CALIPSO Cloud Product
ICNC	Ice Crystal Number Concentration
INP	Ice-Nucleating Particle
INPC	Ice-Nucleating Particle Concentration
IPCC	Intergovernmental Panel on Climate Change
IWP	Ice Water Path
LCL	Lifting Condensation Level
LES	Large-Eddy Simulation
LWP	Liquid Water Path
MOSAiC	Multidisciplinary drifting Observatory for the Study of Arctic Climate
MPC	Mixed-Phase Cloud
PIN	Primary Ice Nucleation
RCM	Regional Climate Model
SCE	Stochastic Collection Equation
SIP	Secondary Ice Production
WBF	Wegener-Bergeron-Findeisen

List of symbols

a	Parameter in hydrometeor diameter-mass relationship
A	Number density of asperities susceptible to breaking
A_0	Normalization factor in generalized gamma distribution
b	Parameter in hydrometeor diameter-mass relationship
C	Capacitance
C_A	Asperity-fragility coefficient
D, D_r	Diameter of hydrometeor, raindrop
D_v	Diffusivity of water vapor in air
DE	Dimensionless energy (mode 2 of drop shattering parameterization)
e	Partial pressure of water vapor in air
e_D	Partial pressure of water vapor over a spherically curved water surface
e_i	Saturation vapor pressure over ice
e_w	Saturation vapor pressure over water
$e_w(D)$	Saturation vapor pressure over a water droplet of diameter D
e^o	Saturation vapor pressure over flat surface
$f(m)$	Mass distribution function
F_{BR}	Number of fragments produced per collision in collisional breakup parameterization
F_{DS_1}	Number of fragments produced by mode 1 of drop shattering parameterization
$f_{DS_2}(T)$	Fraction of droplets already frozen initially due to supercooling (mode 2 of drop shattering parameterization)
F_{DS_2}	Number of fragments produced by mode 2 of drop shattering parameterization
$f_{RS}(T)$	Limiting factor in rime splintering parameterization
F_{RS}	Number of fragments produced from rime splintering
$\bar{f}_h$	Mean ventilation coefficient for heat diffusion
$\bar{f}_v$	Mean ventilation coefficient for vapor diffusion
K	Collection kernel
K_0	Collisional kinetic energy
k_a	Heat conductivity of air
L_e	Latent heat of evaporation of water
L_m	Latent heat for melting of ice

m	Mass
m_{ice}	Ice mass
m_{rime}	Mass of rime on a frozen hydrometeor
M_w	Molecular weight of water
N, N_c, N_i	Number concentration of hydrometeors, cloud droplets, ice crystals
n_s	Number of solute moles
Q, Q_c, Q_i	Mass mixing ratio of hydrometeors, cloud droplets, ice crystals
r	Droplet radius
R	Universal gas constant
S	Saturation ratio
t	Time
T	Temperature
T_0	Freezing temperature, $T_0 = 273.15$ K
v	Terminal fall velocity of hydrometeor
α	Parameter in hydrometeor fall speed-mass relationship
α_h	Equivalent-spherical surface area of the smaller, fracturing hydrometeor
β	Parameter in hydrometeor fall speed-mass relationship
γ	Parameter in hydrometeor fall speed-mass relationship
γ_r	Parameter in collisional breakup equation depending on the rimed fraction and hydrometeor type
Γ	Euler gamma function
ζ	Coefficient depending on D_r for mode 1 of drop shattering parameterization
η	Coefficient depending on D_r for mode 1 of drop shattering parameterization
λ	Slope parameter in generalized gamma distribution
μ	Shape parameter in generalized gamma distribution
ν	Shape parameter in generalized gamma distribution
$\Xi(D_r)$	Cubic interpolation function for mode 1 of drop shattering parameterization
ρ	Air density at a specific altitude
ρ_0	Air density at sea level
$\rho_v(D)$	Density of water vapor at the surface of a droplet
$\rho_{v,s}$	Density of water vapor at the surface of an ice crystal
$\rho_{v,\infty}$	Bulk density of water vapor
ρ_w	Density of water
σ_w	Water surface tension
ϕ	Coefficient depending on D_r for mode 1 of drop shattering parameterization
$\Phi(T)$	Empirical probability that a produced secondary droplet contains ice (mode 2 of drop shattering parameterization)
$\Omega(T)$	Cubic interpolation function for mode 1 of drop shattering parameterization

Part I

Introductory chapters

Chapter 1

Clouds in the climate system

Clouds are ubiquitous in most locations on Earth, except for regions characterized by persistent large-scale descending air, such as the Sahara in Northern Africa (see Fig. 1.1). As vital components of the water cycle, they transport moisture and energy and act as a precipitation source. Their interaction with both the incoming shortwave (solar) radiation and outgoing longwave (terrestrial) radiation further impacts the global energy balance. Beyond these effects, the surface of cloud droplets and ice crystals can catalyze chemical

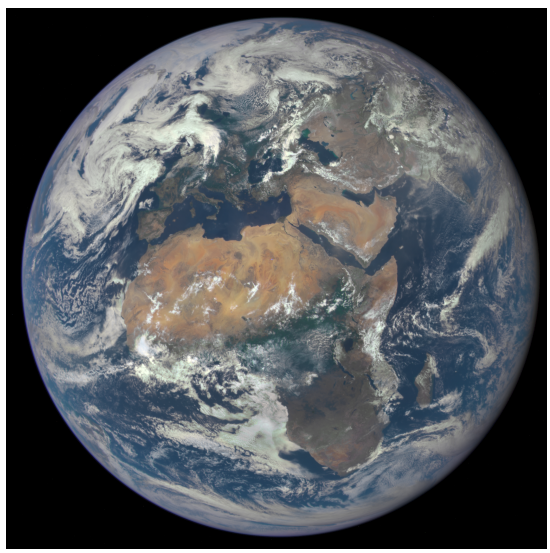

Figure 1.1: Earth, picture by NASA's Deep Space Climate Observatory (DSCOVR) satellite.
Image credit: NASA

reactions in the atmosphere that, e.g., form ozone-depleting substances in the polar stratosphere, which caused the Antarctic ozone hole (e.g., Solomon, 1988).

Even though clouds are vital for the global climate, there are still large uncertainties regarding how they affect and are affected by climate change (IPCC, 2021). This is because many factors influence cloud properties, leading to different climatic effects. Indeed, cloud-related uncertainties are the most important source of uncertainty in how future climate will respond to anthropogenic impacts (Zelinka et al., 2020).

One important cloud property that impacts macrophysical cloud structure, precipitation formation, and cloud radiative effect, is whether a cloud consists of liquid droplets (liquid cloud), ice crystals (ice cloud) or a mixture of both (mixed-phase cloud). As difficult as single-phase clouds are to model, mixed-phase clouds pose an even larger challenge. The coexistence of liquid and frozen water is thermodynamically unstable. Additionally, many small-scale interactions between liquid and frozen hydrometeors[1] need to be represented; these are referred to as cloud microphysics (Chapter 4). The challenge of modeling mixed-phase clouds, with a focus on the ice phase, has been the primary motivation behind the research presented in this thesis.

1.1 Cloud formation and cloud types

Clouds form when air becomes saturated, typically because moist air is lifted. The lifting can be caused by convection, large-scale vertical motions during the passage of a frontal system, or by topography such as mountains. As an air parcel rises, it cools dry-adiabatically by about 1 °C per 100 m. Due to this cooling, the saturation vapor pressure e_s decreases (Pruppacher and Klett, 2010). When the actual vapor pressure equals e_s, saturation is reached at the so-called lifting condensation level (LCL) forming the cloud base. However, the formation of cloud droplets requires the presence of aerosol particles to act as cloud condensation nuclei (CCN) which allow water vapor to condense at minimal supersaturations. The resulting phase change releases latent heat into the rising air parcel, causing it to cool at the slower, moist-adiabatic rate of typically 0.5-0.7 °C per 100 m. By cooling at this reduced rate, the parcel remains warmer and less dense than the surrounding environment, allowing it to keep rising. Once the air parcel reaches a level with the same density as the surrounding air—for example, due to a temperature inversion—the parcel ceases to rise. This is the cloud top.

Different cloud types result from the interplay between the initial lifting mechanism and the broader thermodynamic structure of the atmosphere. Convective lifting causes cumulus clouds to form, which have a defined bottom and fluffy, often well-defined outlines (Fig. 1.2a). These clouds can consist of both liquid droplets and frozen ice crystals, yet the majority contain liquid droplets that cause the well-defined edges. Cumulus clouds often have a short

[1] Literally translated from Greek as "water suspended in the air", defined as any liquid or frozen water in the atmosphere.

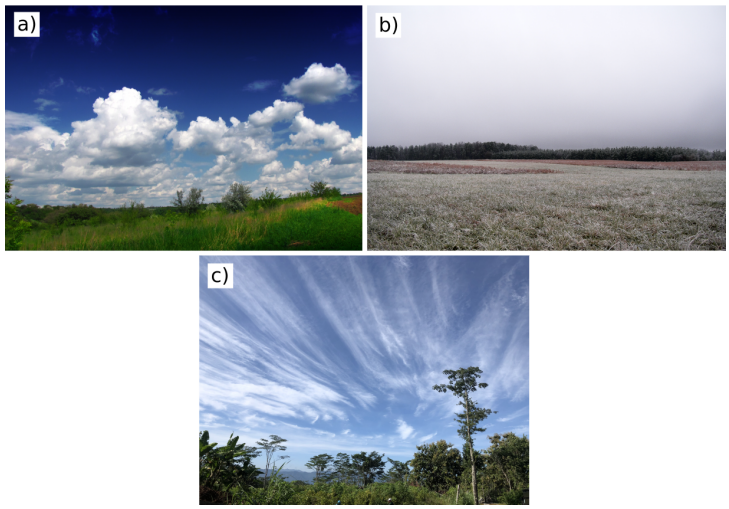

Figure 1.2: Different cloud types: a) cumulus, b) stratus, and c) cirrus. Image credit: Wikimedia Commons

lifetime of less than one hour (Cotton et al., 2010) and can produce rain or snow showers.

Forced lifting by large-scale air motions or topography tends to form stratiform clouds (Fig. 1.2b). These are much larger in the horizontal than in the vertical dimension and often form a closed layer. Stratiform clouds can consist of liquid droplets or frozen ice crystals, as well as a mixture of both, and can produce light precipitation. The lifetimes of these clouds range from 6 to 12 hours (Cotton et al., 2010).

Finally, both convective and forced lifting can cause cirrus clouds to form. They are high clouds consisting solely of ice crystals, which makes them almost transparent to sunlight and gives them a feather-like appearance (Fig. 1.2c). They often have blurry edges due to ice crystals slowly sedimenting out of the cloud (Penner et al., 1999). These sedimenting ice crystals sublimate in drier air, preventing the formation of surface precipitation. Cirrus can form in deep convection as anvil clouds on top of thunderstorms, but in the mid-latitudes they form due to forced lifting. They have typical lifetimes of several hours.

1.2 The role of aerosol particles

As mentioned above, aerosol particles are required for water vapor to condense once the air has reached saturation (see Sect. 4.3 for details). In most parts of the troposphere, enough aerosol particles are available to facilitate the condensation of all water vapor exceeding the saturation pressure, with aerosol concentrations ranging from 300 to 10.000 cm^{-3} (Spracklen et al., 2010).

Additionally, aerosol particles play an important role regarding the freezing of cloud droplets to ice crystals. At temperatures between 0 and approximately

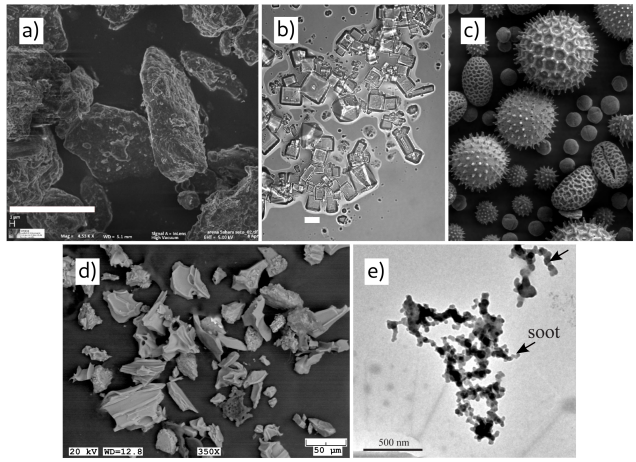

Figure 1.3: Scanning electron microscopy images of different aerosol types: a) Sahara desert dust, b) sea salt, c) pollen, d) volcanic ash, and e) soot. The white bars in a) and b) mark 1 and 15 µm, respectively, the black bars in d) and e) illustrate 50 µm and 500 nm, respectively.
Full attribution is provided in the list of figures.

-38 °C, specific aerosol particles, so-called ice-nucleating particles (INPs), are necessary to cause a supercooled cloud droplet to freeze (heterogeneous ice nucleation, see Sect. 4.4 for details). Only a small subset of atmospheric aerosol particles can act as INPs, so their abundance can determine whether a cloud remains liquid, develops into a mixed-phase cloud, or glaciates entirely into an ice cloud. Whether an aerosol particle can act as an INP depends, among other factors, on its type and size.

Many different types of aerosol particles exist: mineral dust or sea salt particles suspended by wind, biological aerosol particles released by plants or microorganisms, ash and dust from volcanic eruptions or wildfires, and dust, soot, organic, and inorganic aerosol particles released by human activities like combustion, industrial processes, or agriculture (Fig. 1.3). The size of aerosol particles spans many orders of magnitude, from a few nanometers (10^{-9} m) to several tens of micrometers (10^{-5} m). Aerosol size influences, together with typical removal processes, the atmospheric lifetime, which ranges from hours to months, but is typically a few days to weeks. The most common removal processes are dry deposition (which includes gravitational settling for the largest particles and turbulent transport for smaller particles) and wet deposition. Wet deposition refers to the removal of aerosol particles falling to the surface with a precipitating hydrometeor. This can occur either through in-cloud scavenging, where an aerosol particle is incorporated into a cloud droplet or ice crystal (e.g., by acting as CCN or INP) that subsequently grows into precipitation, or through below-cloud scavenging, where falling hydrometeors collect particles from the air beneath the cloud base.

1.3 Clouds and the global energy balance

Clouds interact with both outgoing longwave and incoming shortwave radiation. Figure 1.4 illustrates that their effect on radiation depends strongly on the height and temperature of the cloud, as well as the phase of the hydrometeors. Low clouds reside in the warmest regions of the atmosphere and therefore primarily manifest as liquid clouds. Cloud albedo (shortwave reflectivity) increases with the amount of liquid water and the number of liquid droplets (Seinfeld and Pandis, 2016), which makes liquid clouds highly reflective to incoming shortwave radiation: they can have an albedo of up to 0.9 (Hartmann, 1994). Low clouds exert only a small greenhouse effect, because the similarity in temperature between low clouds and the surface means there is only a minimal reduction in the longwave radiation escaping to space. For these liquid-dominated low clouds, the net result at the top of the atmosphere is therefore a strong cooling effect (Matus and L'Ecuyer, 2017). High cirrus clouds are almost transparent for shortwave radiation with typical albedos below 0.3 (Fu and Liou, 1993), since they consist of little to no liquid water and ice crystals are much less reflective than liquid droplets. Ice clouds have a considerable greenhouse effect, because they reside at altitudes with low temperatures. Due to their low temperature, ice clouds emit significantly less longwave radiation toward space than the warmer underlying surface or the cloud-free atmosphere. This causes a strong greenhouse effect because the trapped radiation is kept within the atmosphere. Overall, ice clouds have a net warming effect at the top of the atmosphere (Matus and L'Ecuyer, 2017).

Another important aspect of the radiative effect of a cloud is the albedo of the underlying surface. The lower the surface albedo is, the higher the shortwave effect of the cloud becomes. This means that low-level clouds have

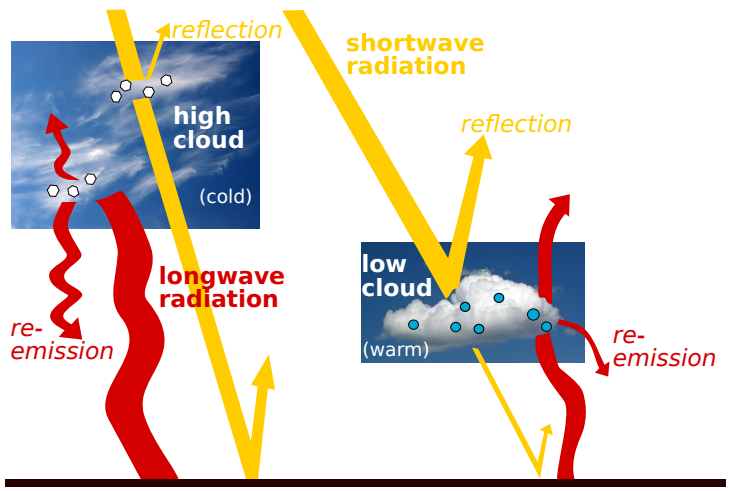

Figure 1.4: The impact of clouds on radiation.
Image credit: Luisa Ickes, incorporating images by James St. John, via Wikimedia Commons

a larger shortwave effect over dark surfaces like open ocean than over highly reflective ice or snow. Indeed, low-level clouds in polar regions have a net warming effect at the surface through most of the year due to the high surface albedo and low solar elevation (Shupe and Intrieri, 2004).

Beyond their radiative impacts, clouds release latent heat through the condensation and freezing of water vapor. By releasing the energy originally absorbed during surface evaporation, these phase changes drive the transport of heat, forming another fundamental component of the global energy balance.

1.4 Observing clouds

Accurate and comprehensive cloud observations provide the foundation for understanding cloud-climate interactions and for the development, initialization, and evaluation of numerical models. These observations must characterize cloud occurrence, vertical structure, and phase partitioning, as well as the variability in hydrometeor size distributions and number concentrations. Different observing systems are employed to provide these measurements, ranging from satellite- and ground-based remote sensing to in situ observations and balloon-borne radiosondes. Satellite remote sensing offers broad spatial coverage, but retrievals are indirect and are limited in spatial and, depending on the platform, temporal resolution. Ground-based remote sensing typically has high spatial and temporal resolution, but limited spatial coverage. In situ measurements (e.g., from aircraft or radiosondes) offer the highest spatial and temporal resolution but are episodic and spatially limited. Radiosondes provide vertical profiles of temperature, humidity, and wind that characterize the thermodynamic environment in which clouds form. They have very high vertical resolution, but varying spatial and temporal coverage.

Remote sensing observations, from satellites and from the ground, use either active or passive sensors. Active sensors emit pulses of electromagnetic radiation and measure the backscattered signal from objects in the atmosphere such as hydrometeors or aerosol particles. The time delay between transmission and reception provides the distance of the scattering object. Thus, active remote sensors enable cloud occurrence retrievals with high vertical resolution. Retrieval algorithms provide information like water content, hydrometeor fall velocities, and even hydrometeor size distributions. Polarization measurements can further constrain the shape and phase of hydrometeors. The choice of wavelength is likewise critical and depends on the hydrometeor size; smaller scatterers require shorter wavelengths. Lidars operate at short wavelengths in the visible/near-infrared, whereas atmospheric radars use microwave wavelengths. One example of an active remote sensing instrument is the Cloud and Aerosol Lidar with Orthogonal Polarization (CALIOP) onboard the CALIPSO (Cloud-Aerosol Lidar and Infrared Pathfinder Satellite Observations) satellite. CALIOP provides vertical profiles of aerosol particle occurrence and cloud fraction, including information on cloud phase (Winker et al., 2009). We compared a dataset based on CALIOP to output from three General Circulation Models (GCMs) in Paper 2.

Passive sensors measure solar radiation reflected by clouds and thermal radiation emitted by clouds, the atmosphere, or the Earth. Cloud properties such as cloud presence, cloud-top or cloud-base temperature, and integrated water measures can then be inferred through radiative transfer calculations and retrieval algorithms. For example, microwave radiometers retrieve the vertically integrated liquid water content, Liquid Water Path (LWP), used for model evaluation in Paper 1 and 3.

Radiosondes are balloon-borne instruments that measure profiles of pressure, temperature, humidity, and horizontal wind from the surface to an altitude of 10 to 30 km. These profiles describe the thermodynamic state of the atmosphere and can be used to identify moist, possibly cloudy layers, and inversions relevant for cloud formation and persistence. Applying thermodynamic relationships, radiosonde profiles can be used to estimate the LCL and to diagnose convective potential, which is related to the likelihood of convective showers and thunderstorms. The simulations in Paper 1 and 3 were initialized with profiles observed by radiosondes. These directly observed profiles are crucial for establishing baseline atmospheric conditions, but exploring how these localized states evolve over time motivates the use of numerical models.

Chapter 2

Atmospheric modeling frameworks

Observations provide the essential empirical foundation for understanding cloud behavior, yet they are inherently limited in spatial and/or temporal resolution. To bridge these gaps, atmospheric science relies heavily on numerical models. These frameworks combine theory with empirical data to investigate the lifecycle of clouds and their broader atmospheric impacts. The research presented in this thesis used models across scales to investigate cloud processes.

2.1 Overview of atmospheric numerical models

Numerical models of the Earth system are based on the fundamental conservation of momentum, mass, and energy. The equations describing the conservation laws, like the equations of motion, generally have no analytical solution. Instead, they require numerical solutions to calculate the evolution of prognostic variables in both time and space. These numerical methods vary between models and require a discretization of the continuous equations onto a computational grid. A primary distinction between models is the spatial and temporal model resolution, which spans a wide range of scales. General Circulation Models (GCMs) or Earth System Models (ESMs) that are used for climate projections typically use grid spacings of approximately 100 km at the equator. In contrast, limited area models, such as Regional Climate Models (RCMs), employ finer grid spacings of 5-50 km, while Large-eddy simulations (LES) can have grid spacings as small as a few meters. Figure 2.1 illustrates the resolution differences: the GCM averages cloud water over a 100 km $\times$ 100 km grid box, effectively obscuring any fine-scale spatial variability. In contrast, the 62.5 m $\times$ 62.5 m grid spacing of the LES explicitly resolves the largest turbulent eddies, making the resulting cloud water minima and maxima clearly distinguishable.

Due to the resolution constraints, physical processes occurring at scales smaller than the grid spacing cannot be resolved and must be parameterized.

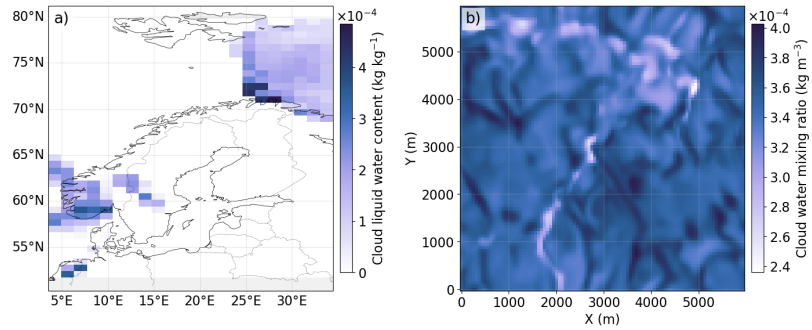

Figure 2.1: Cloud liquid water fields at a single model time step simulated by a) the IPSL-CM6A-MR1 GCM (Boucher et al., 2023) and b) the MIMICA LES. The GCM data have a horizontal resolution of 100 km, whereas the LES data use a 62.5 m grid spacing.

This approach involves describing sub-grid processes using variables that are explicitly resolved on the model grid. Parameterizations are typically grounded in observations or theoretical considerations. For instance, the freezing of cloud droplets occurs at scales far below the grid resolution of all aforementioned models. Consequently, this process is often parameterized as a function of the resolved temperature. The specific processes requiring parameterization depend on the model grid resolution. Turbulence must be parameterized in GCMs; in contrast, LES models are designed to resolve the largest turbulent eddies explicitly (Fig. 2.1). However, cloud microphysics always requires parameterization, as fundamental processes such as droplet activation or hydrometeor collisions occur on scales much smaller than the spatial resolution of any current atmospheric model.

2.2 General circulation models

This description is restricted to atmospheric general circulation models. In this setup, as used in Paper 2, the ocean and cryosphere are not dynamically coupled to the atmosphere, but instead represented through prescribed sea surface temperatures and sea ice concentrations. GCMs represent fundamental atmospheric physics, including large-scale dynamics, the interaction of solar and terrestrial radiation with the atmosphere, and the evolution of clouds, chemistry, and aerosol particles. A primary application of GCMs is the projection of future climate states, although they are also widely used for process understanding and attribution studies. Researchers frequently conduct sensitivity experiments to evaluate GCM performance and identify the physical drivers of model behavior. By isolating or modifying specific processes, as demonstrated in Paper 2, the influence of individual components on the simulated climate can be assessed.

GCMs often reach a high degree of structural complexity, because they typically are developed through extensive international collaborations and include a multitude of physical processes. However, this complexity requires

careful evaluation to ensure that the represented processes are necessary and physically consistent. For instance, Paper 2 demonstrates that for one of the investigated models, only one of the four ice-related processes exerted a relevant impact on the cloud phase. This suggests that the remaining three mechanisms may be computationally redundant in certain contexts. Such findings are vital because available computational power strictly limits both model resolution and the level of detail that can be represented.

GCMs explicitly resolve large-scale atmospheric dynamics—such as extratropical cyclones and planetary waves—by integrating the equations of motion together with conservation laws for mass and energy. Sub-grid processes that must be parameterized include turbulence, cloud microphysics, aerosol processes, radiation, and chemistry. Parameterizations represent a major source of uncertainty in GCMs, as they may only be valid for specific temperature ranges, rely on incomplete theoretical understanding, or engage in unexpected interactions with other model components (Goosse et al., 2008). The structural diversity of parameterizations is a primary cause of persistent GCM divergence and—as concluded in Paper 2—limits the capacity of any single model to provide universal insights into the global climate system. This model divergence is evident in the CMIP6 (Coupled model intercomparison project phase 6) ensemble, which exhibits both an increased spread and a higher average magnitude of climate sensitivity[1] compared to the CMIP5 predecessor (Zelinka et al., 2020). Much of this shift originates from the representation of clouds, which is generally divided into two distinct schemes in GCMs. Stratiform clouds are associated with large-scale ascent and humidity resolved on the model grid; however, the phase changes and precipitation processes within these clouds must be parameterized through a microphysics scheme. In contrast, convective clouds occur at scales significantly smaller than the grid box and are represented by a convection parameterization that describes vertical transport and cloud formation within a sub-grid column. This artificial separation between stratiform and convective processes has long been recognized as a fundamental limitation in atmospheric modeling (Arakawa, 2004). Identifying how specific processes in the stratiform cloud scheme influence the resulting cloud phase served as a primary motivation for the process study conducted in Paper 2.

The inherent limitations of GCMs, particularly regarding sub-grid parameterizations and the artificial separation between cloud types, motivate the use of high-resolution models to gain a more detailed understanding of the underlying physical processes. Large-eddy simulations (LES) use much finer grid spacings, and thus they can explicitly resolve the largest turbulent eddies that GCMs must approximate through parameterization (Fig. 2.1). By resolving these motions, LES provides a more detailed representation of the coupling between small-scale atmospheric dynamics and microphysical processes. This capability allows for a more rigorous investigation of the mechanisms governing cloud phase and serves as a tool to evaluate the physical assumptions and parameterizations used in coarser models.

[1]The change in global mean surface temperature following a doubling of CO_2

2.3 Large-eddy simulation models

Atmospheric LES models are high-resolution frameworks typically used to investigate clouds, convection, or turbulence within limited domains, often spanning less than 100 km. By operating with high spatial resolutions that reach horizontal scales of only a few meters, these models can bridge the gap between small-scale atmospheric observations and modeling, as demonstrated in Paper 3. The high resolution allows for the direct representation of the largest turbulent eddies, whereas GCMs must approximate these motions through parameterizations. Consequently, LES serves as a testbed for parameterizations that may be implemented in larger-scale models like GCMs, as shown in Paper 1.

A primary advantage of this high resolution is that LES does not require the artificial separation between stratiform and convective cloud schemes. The resolution of vertical motions is sufficient to permit the application of a unified microphysics parameterization across all cloud types. However, processes occurring at scales smaller than the grid, such as sub-grid scale turbulence and cloud microphysics, still require parameterization. Unlike GCMs, LES models operate on a limited area where the boundaries must be constrained. Large-scale flow and advection can be provided by a coarser driving model or reanalysis data, while an alternative approach involves periodic boundary conditions. In this setup, the total mass in the domain is conserved by allowing air flowing out of one boundary to re-enter on the opposite side, a method employed in Paper 1 and Paper 3.

The LES model used in this thesis is MIMICA (MISU/MIT Cloud-Aerosol model), as described in Savre et al. (2014). It solves the anelastic, nonhydrostatic equations of motion alongside conservation equations for mass, potential temperature, and total water content in three dimensions. MIMICA was developed primarily to investigate high-latitude mixed-phase clouds (e.g., Savre and Ekman, 2015; Stevens et al., 2018; Sotiropoulou et al., 2020), though it has also been applied to studies of mid-latitude marine stratocumulus (e.g., Bulatovic et al., 2019) and deep convective clouds (Bardakov et al., 2020). The following description details the model version used in Paper 3. It should be noted that Paper 1 employed a previous model version which featured significant differences in the microphysical parameterization.

MIMICA employs a two-moment bulk microphysical scheme (Seifert and Beheng, 2006) that prognoses the number concentration and mixing ratio of the five hydrometeor types cloud droplets, raindrops, ice crystals, snow, and graupel (see Chap. 4 for details). The scheme assumes cloud droplets do not sediment until they reach a diameter of 40 μm, at which point they are classified as falling raindrops. Snow represents the aggregation of individual ice crystals. Graupel, by contrast, is generated when liquid droplets rime onto frozen hydrometeors. The microphysical parameterization accounts for condensation, evaporation, sublimation, autoconversion, accretion, aggregation, melting, and riming. Under supersaturation, condensation to cloud droplets and deposition to ice crystals are calculated according to Pruppacher and Klett (2010). Radiation calculations are based on a framework including both shortwave and longwave frequencies (Fu and Liou, 1993; Fu et al., 1997; Gu

et al., 2003). Only cloud liquid interacts with radiation. This radiative effect is determined by the mixing ratios and effective radii of cloud droplets and raindrops, whereas cloud ice does not affect radiation.

The recent Cold-Air Outbreaks in the Marine Boundary Layer Experiment (COMBLE) intercomparison (Juliano et al., 2026) provides an ideal opportunity to contextualize MIMICA alongside other prominent LES models by simulating the evolution of an Arctic convective mixed-phase cloud. The participating LES models include WRF (Skamarock et al., 2019), DHARMA (Stevens, 2002), SAM (Khairoutdinov and Randall, 2003), DALES (Heus et al., 2010), ICON-LEM (Dipankar et al., 2015), MSU-INM LES (Mortikov et al., 2019; Kadantsev et al., 2021; Voevodin et al., 2023), CM1 (Bryan and Fritsch, 2002; Morrison and Milbrandt, 2015), SCALE (Nishizawa et al., 2015), UCLALES-SALSA (Stevens et al., 1999; Stevens et al., 2005; Stevens and Seifert, 2008), and MIMICA (Savre et al., 2014) in a similar version as in Paper 3. Eight of these ten frameworks employ two-moment bulk microphysical schemes similar to MIMICA, with the majority using the identical parameterization by Seifert and Beheng, 2006. Six of the models explicitly account for radiation interactions with cloud ice, in contrast to MIMICA which restricts interactions to the liquid phase. For the mixed-phase case in the COMBLE intercomparison, MIMICA simulated latent and sensible heat fluxes near the median of the LES ensemble spread, but the lowest ice water path (IWP), surface precipitation, cloud cover, and cloud optical depth among all participating LES models. Consequently, the reduced cloud cover and optical depth caused MIMICA to compute the highest outgoing longwave radiation at the top of the atmosphere and lowest downward longwave radiation at the surface (Juliano et al., 2026). Although the majority of the LES models use the identical base microphysics parameterization, this pronounced divergence of cloud cover and optical depth indicates that the simulated cloud is sensitive to specific implementation choices and interactions with other parts of the model. Understanding how these microphysical sensitivities impact cloud evolution—particularly in Arctic mixed-phase clouds—provides a primary motivation for the research presented in this thesis.

Chapter 3

Arctic clouds

Although Arctic clouds are governed by the same fundamental physical mechanisms valid globally, the extreme and highly coupled nature of the local climate system significantly alters their evolution. To understand why simulating these specific mixed-phase clouds remains so challenging, it is first necessary to examine the unique environmental conditions that define the region.

3.1 Arctic climate

Polar environments are characterized by extreme seasonal differences in solar insolation: during polar summer, the sun never sets, while it remains below the horizon throughout polar winter. Additionally, the poles are covered with ice and snow, resulting in high surface reflectivities. Exceptions include open leads, polynyas, or entirely open ocean areas, which exhibit very low albedo.

Antarctica is a continent, whereas the Arctic consists of an ocean basin surrounded by landmasses. This geographical difference fundamentally shapes the atmospheric circulation, environmental conditions, and the distinct character of the polar ice masses. Antarctica is covered by a continental ice sheet surrounded by sea ice, while in the Arctic, only Greenland is covered by an ice sheet, with the remaining ice consisting of sea ice. These polar contrasts likely explain why the Arctic, in particular, warms at a rate far exceeding the global average (Goosse et al., 2018; Rantanen et al., 2022), so-called Arctic amplification. The rapid transformation of the Arctic climate system motivates the investigation of cloud processes in this sensitive region.

The unique physical state of the polar atmosphere represents a primary component of this susceptibility. Low surface temperatures at high latitudes dictate a low absolute water vapor content, due to the temperature dependency of the saturation vapor pressure. Although the absolute water vapor content is low, relative humidity is generally high throughout the polar atmosphere because of the low saturation vapor pressure. Apart from ice-free land or open ocean areas, the Arctic lacks significant local aerosol sources.

3.1.1 Arctic amplification

The Arctic is strongly affected by global climate change. Temperatures in the Arctic have increased significantly faster than the global average (see Fig. 3.1). Connected to this Arctic amplification, sea ice has retreated substantially in recent decades, as shown in Fig. 3.2, which illustrates the negative trend in annual minimum sea ice extent. Furthermore, Fig. 3.3 shows the second lowest minimum Arctic sea ice extent observed on 15 September 2020, compared to the median extent of 1981-2010. The sea ice covered an area equivalent to only 62 % of the 1981-2010 September average. Several processes are hypothesized to contribute to Arctic amplification (e.g., Serreze and Barry, 2011):

- Albedo feedback: With initial warming, ice and snow will melt faster or earlier than in previous years. The exposed land or sea surface has a lower albedo than ice or snow and absorbs more incoming shortwave radiation. This absorption warms the surface and the lower atmosphere, enhan-

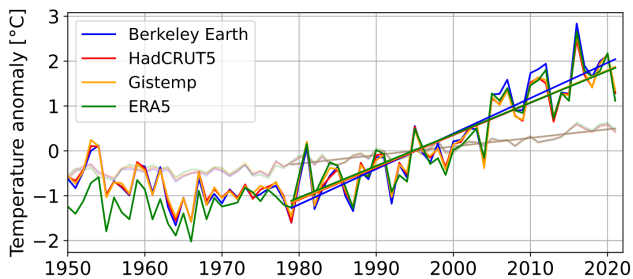

Figure 3.1: Temperature anomalies averaged globally (light beige) and across the Arctic according to different observational datasets. Anomalies were calculated relative to the 1981-2010 averages.
Image credit: Rantanen et al. (2022)

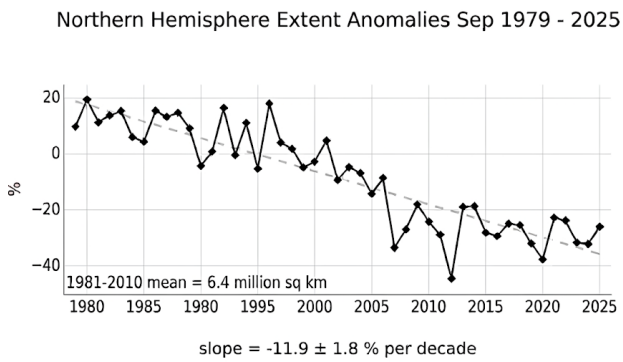

Figure 3.2: Time series of average September Arctic sea ice extent anomalies relative to the 1981 to 2010 average. The linear trend indicated is -11.9 % per decade.
Image credit: National Snow and Ice Data Center (2026, modified)

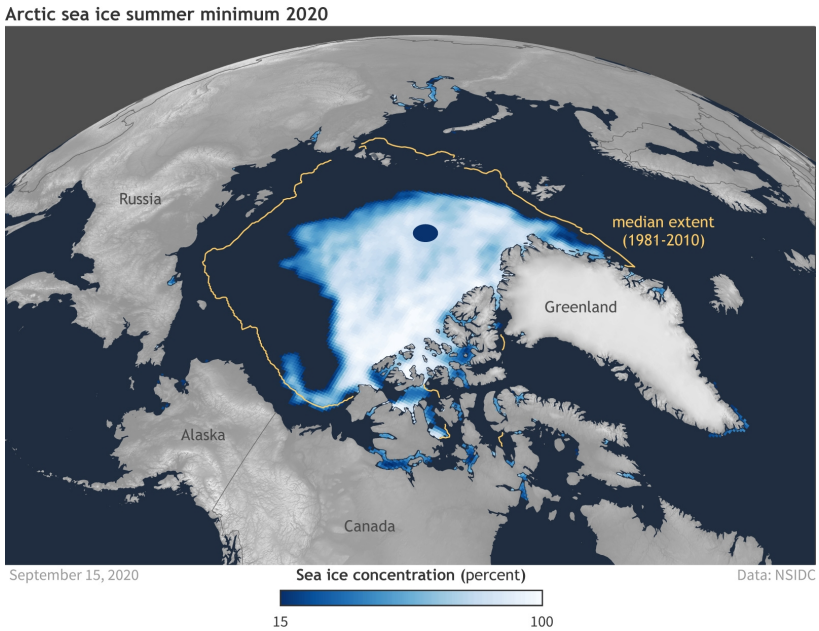

Figure 3.3: Arctic sea ice extent on 15 September 2020. The 2020 minimum represents the second-lowest extent recorded since 1979.
Image credit: National Oceanic and Atmospheric Administration (NOAA) climate.gov (2020)

cing melting in surrounding areas and creating a positive (amplifying) feedback.

- Sea ice loss: Sea ice insulates the relatively warm ocean from the cold atmosphere. As sea ice extent decreases due to initial warming, more heat is transferred from the ocean to the lower atmosphere, resulting in additional warming and further melting. This results in a positive feedback.

- Horizontal heat fluxes: Increased atmospheric heat fluxes to the Arctic free troposphere contributed significantly to the decadal warming trend between 1992 and 2008 (Yang et al., 2010). In the ocean, heat advection also drives warming in the Arctic (Serreze and Barry, 2011). Both increases in poleward heat flux are primarily driven by decadal variations in atmospheric and ocean circulations rather than anthropogenic emissions, yet they contribute to enhanced Arctic warming.

- Water vapor: Increased water vapor in the Arctic atmosphere enhances longwave emissions toward the surface, leading to surface warming. From 1989 to 2008, water vapor content in the Arctic has increased, with much of this change attributed to sea ice loss and subsequent evaporation from the underlying ocean (Screen and Simmonds, 2010). General warming in

the Arctic and the resulting increase in saturation vapor pressure also contribute to the rising water vapor content.

- Clouds: Clouds exert a surface warming effect in the Arctic during most of the year (e.g., Philipp et al., 2020; Arouf et al., 2024). Increasing cloud cover, especially for low-level clouds, would therefore enhance warming. Additionally, changes in the microphysical structure of clouds are important and increases in liquid water content enhance longwave emissions toward the surface. A shift toward the liquid phase could be amplified by warming, since the altitudes where cloud ice can form increase. Observational studies have reached differing conclusions regarding seasonal and regional cloud changes (e.g., Wang and Key, 2005; Eastman and Warren, 2010; Philipp et al., 2020), and also the latest assessment report by the IPCC (Intergovernmental Panel on Climate Change) summarizes that the Arctic cloud feedback is only slightly more likely to be positive than negative (IPCC, 2021). This uncertainty regarding their true radiative effect serves as a primary motivation for investigating Arctic clouds.

3.2 Clouds in the Arctic

3.2.1 Physics of Arctic clouds

Clouds have been observed at various Arctic locations during the majority of the year, with a minimum cloud abundance in winter and a maximum in late summer/fall (Shupe et al., 2011). The lower the altitude, the higher their abundance (Shupe et al., 2011).

The specific features of the Arctic climate as described in Sect. 3.1 affect the conditions for clouds. Due to the lower temperatures, ice potentially dominates in clouds. The typically low aerosol concentrations on the other hand limit heterogeneous cloud ice formation between 0 and -38 °C. As a consequence, entirely liquid clouds can be observed down to -24 °C in the Arctic (Shupe, 2011). However, ice clouds are the dominant cloud phase in the Arctic, followed by mixed-phase clouds (Shupe, 2011).

The strong seasonality of solar radiation in polar regions and the surface properties have large effects on the shortwave Arctic surface energy balance: during winter, the solar part of the energy balance disappears. The lower the solar elevation, the lower becomes the surface cooling effect of clouds by reflecting incoming solar radiation (Shupe and Intrieri, 2004). The cooling effect increases for decreasing surface albedo, with clouds shielding solar radiation from being absorbed by the darker ocean surface. In the Arctic, both of these surface cooling effects lead to a negative net cloud radiative effect only in mid-summer when the highest solar elevation and most open ocean area occur. The positive longwave cloud radiative effect at the surface dominates most of the year and is mainly caused by clouds with a base below 500 m (Shupe and Intrieri, 2004). At this low altitude, the relatively warm cloud base drives significant longwave emission. Furthermore, the frequent temperature inversions often result in low clouds being warmer than the underlying surface

(Shupe and Intrieri, 2004). The magnitude of this warming effect is highly sensitive to the cloud water content (Shupe and Intrieri, 2004).

Due to their warming effect, Arctic clouds govern the Arctic surface energy balance, which controls the melting and freezing of sea ice. This means that clouds can have a substantial impact on the cycle of sea ice formation and melting, and thus on Arctic amplification. On the other hand, changes due to Arctic amplification impact Arctic clouds, especially due to more available water vapor and changes in the thermodynamic vertical structure of the Arctic, as well as changes in aerosol particles acting as CCN or INPs.

3.2.1.1 Implications of the Arctic boundary layer

The Arctic boundary layer (BL) structure varies significantly throughout the year, yet it is predominantly characterized by the presence of temperature inversions. This is supported by recent findings from the Multidisciplinary drifting Observatory for the Study of Arctic Climate (MOSAiC, Shupe et al., 2022), a year-round expedition conducted between September 2019 and October 2020. Observations from this full annual cycle revealed that at least one temperature inversion was present within the lowest 1 km at all times (Jozef et al., 2024). Distinct seasonal patterns were identified: winter is dominated by a predominantly stable BL with strong, near-surface inversions that restrict vertical mixing. These conditions are primarily driven by long cloud-free periods and the lack of solar radiation, which lead to sustained longwave surface cooling. In contrast, during the summer, stronger and weaker stability cases occur with similar frequency (Jozef et al., 2024).

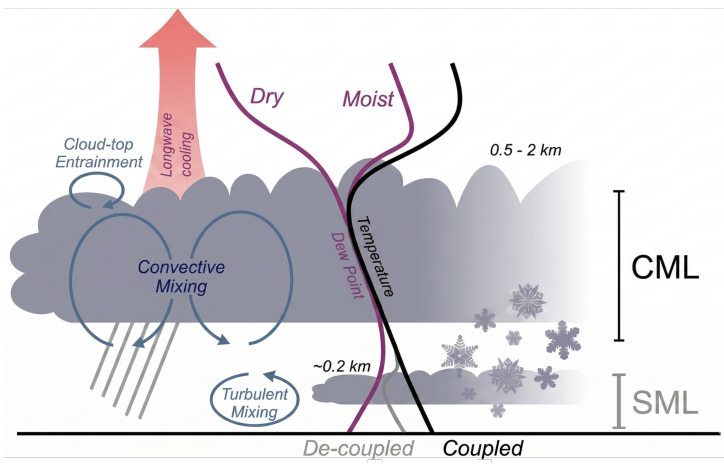

Figure 3.4: Schematic of a typical summertime Arctic boundary layer topped by stratus and its governing processes. CML: cloud mixed layer, SML: surface mixed layer. The gray and black lines represent temperature profiles for surface de-coupled and coupled cases, respectively. The magenta line illustrates the profile of specific humidity.
Image credit: Brooks et al. (2017, modified)

In the summertime Arctic, the structure of the BL is fundamentally shaped by the ubiquitous presence of mixed-phase clouds, which maintain an average cloud fraction of 80-90 % (Curry and Ebert, 1992). At lower latitudes, surface heating typically drives vertical mixing, while in the Arctic summer BL, cloud-top radiative cooling often is the primary source of turbulence (Tjernström et al., 2012). This cooling generates dense, sinking air parcels that drive a top-down mixed layer, providing a critical mechanism for the connection between the BL and the free troposphere (Tjernström et al., 2012) and allowing for the entrainment of moisture or aerosol particles into the BL.

The vertical structure of this system is defined by the interaction between two distinct turbulent regimes (Brooks et al., 2017). At the surface, a shallow well-mixed layer is maintained primarily by wind shear. Above this, the cloud itself drives the second turbulent regime. The overall coupling state of the BL depends not only on the depth and altitude of the cloud-driven mixed layer (Shupe et al., 2013) but also on the stability near the surface (Fig. 3.4). If cloud-generated turbulence reaches low enough to merge with the surface-driven layer, a single, surface-coupled well-mixed BL is formed (Brooks et al., 2017). However, this connection can be blocked if a temperature inversion exists close to the surface, effectively shielding the surface from the cloud-driven mixing. In such cases, the two mixed layers stay separated, and the cloud deck remains decoupled from the surface (Tjernström et al., 2012; Brooks et al., 2017). This decoupling isolates the cloud from surface moisture, making its persistence relying on moisture from above. The relationship between moisture and temperature gradients uniquely defines the Arctic summer BL. Temperature inversions almost universally cap the BL across the globe, yet the Arctic specific humidity profile exhibits a distinctly different behavior. BL clouds at lower latitudes typically reside beneath dry air, whereas the Arctic frequently features a moist layer extending into and even above the temperature inversion (Solomon et al., 2011). This overlying moisture provides a critical reservoir which can help sustain the cloud layer.

3.2.1.2 Low-level stratiform clouds

Low-level clouds are the most abundant clouds in the Arctic from mid-spring to mid-fall (Curry and Ebert, 1992). Many of these low-level Arctic clouds are stratiform and mixed-phase, and they can persist over several hours or even many days (Shupe et al., 2006). This lifetime exceeds that of typical low-latitude stratus clouds (cf. Sect. 1.1), meaning that Arctic mixed-phase stratiform clouds (AMPS) can impact the surface energy balance over an exceptionally long time. Sea ice melting and freeze-up coincide with the highest occurrence of low-level clouds, and thus AMPS can play a critical role in these transition periods.

The vertical structure of AMPS is important for their longevity. Liquid water content often reaches its maximum at the cloud top, and ice crystals precipitate from this liquid layer (Shupe et al., 2008). Ice water content typically increases downwards from the cloud top and peaks near the cloud base; below the cloud most of the ice sublimates before reaching the surface (Shupe et al.,

2008). On average, liquid water dominates the AMPS mass, while ice water content makes up only 15 % of the mass (Shupe et al., 2008).

The dominance of liquid water at the cloud top causes radiative cooling, acting as the main driver for the long persistence of AMPS (e.g., Curry, 1986). The radiative cooling not only causes water vapor to condense, but also generates negatively buoyant downdrafts that sustain turbulence (Morrison et al., 2012). Other important contributors to the longevity of AMPS include the entrainment of aerosol particles and moisture, surface fluxes, and the concentrations of cloud droplets and ice crystals (Morrison et al., 2012). Crucial for the formation of cloud droplets and ice crystals are CCN and INPs. Due to seasonal and often low local aerosol sources, aerosol concentrations can be so low that cloud formation is limited or clouds dissolve once a replenishment of CCN ceases. This is known as the 'CCN-limited' or 'tenuous cloud' regime (Mauritsen et al., 2011). Modeling studies have confirmed that reduced (Stevens et al., 2018; Bulatovic et al., 2023) or removed aerosol concentrations (Sterzinger et al., 2022) can lead to rapid cloud dissipation. Given the scarcity of local sources, aerosol transport from lower latitudes in the free troposphere can be crucial for cloud formation. Year-round lidar data from the MOSAiC expedition confirm that the free troposphere was always well-filled with both CCN and INPs (Jimenez et al., 2025). Surface-based INP observations from MOSAiC suggest that long-range transport is the primary source during winter and late summer (Creamean et al., 2022), yet particles must also be transported from the free troposphere into the BL. Vertical exchange is, at times, facilitated by low-level AMPS reaching into the inversion topping the BL, which allows the clouds to entrain long-range transported aerosol particles from the free troposphere into the BL (Igel et al., 2017). The complex interplay between BL dynamics and microphysics creates significant challenges for numerical models, which frequently struggle to accurately represent AMPS, especially the partitioning between liquid and frozen cloud content (e.g., Birch et al., 2012; Stevens et al., 2018; Zhang et al., 2020; Schäfer et al., 2024). Constraining these model uncertainties and improving phase representations requires comprehensive, long-term observational datasets.

3.2.2 Cloud observations in the Arctic

Although the Arctic region is geographically remote, several permanent atmospheric observation sites provide essential long-term data. These include stations in Ny-Ålesund (Svalbard), Utqiaġvik (Alaska), Eureka and Alert (Canada), and Summit (Greenland). In addition to these land-based sites, several ship-based expeditions have collected valuable datasets above the Arctic Ocean, such as ARTofMELT (May-June 2023; Tjernström and Zieger, 2025), MOSAiC (September 2019-October 2020; Shupe et al., 2022), MOCCHA (August-September 2018; Vüllers et al., 2021), ASCOS (August-September 2008; Tjernström et al., 2014), and SHEBA (October 1997-October 1998; Uttal et al., 2002). The following discussion focuses on the expeditions that provided the underlying data for Paper 1 (ASCOS) and Paper 3 (ARTofMELT).

ASCOS

A primary goal of the Arctic Summer Cloud Ocean Study (ASCOS) was to improve the representation of low-level Arctic clouds in climate models (Tjernström et al., 2014). The campaign featured extensive aerosol observations to characterize the local sources and transport processes of CCN and INPs into cloud-forming regions, as well as the reciprocal impact of clouds on the aerosol population.

Analyses of the ASCOS data drove several important advancements, including the definition of the previously mentioned CCN-limited regime (Mauritsen et al., 2011). Observations from the expedition revealed that low-level clouds were predominantly decoupled from the surface (Sotiropoulou et al., 2014). This decoupling meant that the clouds relied heavily on moisture and aerosols entrained from above to persist (Shupe et al., 2013). The importance of entrainment from above was supported by a MIMICA study, which additionally concluded that sub-cloud droplet evaporation can act as a crucial pathway for transporting free-tropospheric aerosols into the BL (Igel et al., 2017). Finally, surface energy balance analysis showed that clouds mostly had a warming effect at the surface, and the decreasing solar angle combined with increasing surface albedo led to sea ice freeze-up only once significantly fewer low-level clouds were present (Sedlar et al., 2011).

ARTofMELT

The Atmospheric rivers and the onset of sea ice melt (ARTofMELT) campaign aimed to collect a multidisciplinary observational dataset during the transition into the melt season (Tjernström and Zieger, 2025). The primary objective was to capture the interactions within the upper ocean-ice-atmosphere system that lead to the initiation of the sea ice melt. A central hypothesis of the expedition was that atmospheric rivers—narrow corridors of intense poleward heat and moisture transport—provide the initial energy triggering the melting season. To support this, a major goal was the collection of cloud and aerosol particle data not only at the surface, but also through the entire vertical column.

An analysis of vertical observations from one ARTofMELT case study further reinforced the importance of top-down entrainment observed during ASCOS, confirming that the aerosol population at the surface was not sufficient to explain observed cloud droplet concentrations (Pohorsky et al., 2026). Consequently, we initialized the simulations in Paper 3 using a combined aerosol population observed below and above the cloud. This ensured a realistic representation of entraining aerosols, yet our analysis ultimately demonstrated that the simulated cloud was remarkably resilient to aerosol concentrations, only showing sensitivity to variations on the scale of two orders of magnitude. Beyond aerosol availability, the cloud showed pronounced sensitivity to distinct microphysical aspects, notably ice crystal concentration and ice habit.

Chapter 4

Parameterization of cloud microphysics

The microphysical characteristics of hydrometeors, including their size, phase, and shape, fundamentally determine macrophysical cloud properties such as albedo, lifetime, and spatial extent. To represent the microphysical structure of a cloud, the most critical variables are the number concentration and the mass mixing ratio of the various hydrometeor species. Ideally, these variables should be known for the entire size distribution, yet modeling and observational constraints often necessitate the use of bulk values. In a bulk approach, the governing equations for the hydrometeors are integrated over an assumed size distribution, meaning only the total quantities are prognosed.

The microphysical scheme developed by Seifert and Beheng (2006) provides the primary theoretical framework for microphysics within the LES model MIMICA. It separates hydrometeors into the categories cloud droplets, raindrops, ice crystals, snow, and graupel.

4.1 Size distributions of hydrometeors

Hydrometeors within a cloud exhibit a wide range of sizes, which a numerical model must represent. Following the framework by Seifert and Beheng (2006), MIMICA uses mass distributions, $f(m)$, to describe each hydrometeor population. These populations are represented by generalized gamma distributions of the form:

$$f(m) = A_0 m^{\nu} \exp(-\lambda m^{\mu}), \tag{4.1}$$

where A_0 is the normalization factor, λ is the slope parameter, and ν and μ determine the shape of the distribution and depend on the specific hydrometeor category. To derive physical quantities from this distribution, its moments, M^N, are calculated, which are defined as the integrals of the distribution weighted by the n-th power of mass. The 0th and 1st moments are of particular importance, as they correspond to the total number concentration N and the

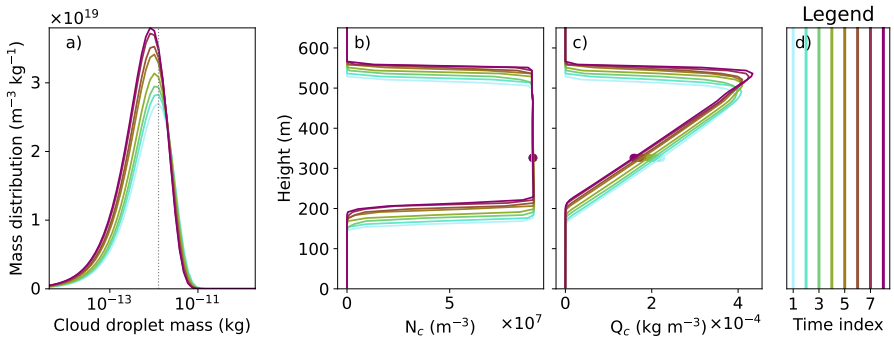

Figure 4.1: Evolution of a) mass distribution $f(m)$, b) number concentration N_c, and c) mixing ratio Q_c of cloud droplets in a cloudy grid box over time (d) of a MIMICA simulation. The mass distribution in a) is shown for the height marked by the dots in b) and c) and the vertical line in a) marks the peak mass at the first time step.

mass mixing ratio Q, respectively:

$$\begin{aligned} M^0 &= \int_0^\infty f(m)dm = N \\ M^1 &= \int_0^\infty mf(m)dm = Q. \end{aligned} \tag{4.2}$$

By substituting Eq. 4.1 into Eq. 4.2, the parameters A_0 and λ can be expressed as functions of N, Q, and the Euler gamma function Γ:

$$\begin{aligned} \lambda &= \left[\frac{\Gamma\left(\frac{\nu+1}{\mu}\right)}{\Gamma\left(\frac{\nu+2}{\mu}\right)} \frac{Q}{N} \right]^{-\mu} \\ A_0 &= \frac{\mu N}{\Gamma\left(\frac{\nu+1}{\mu}\right)} \lambda^{\frac{\nu+1}{\mu}}. \end{aligned} \tag{4.3}$$

A_0 and λ are updated at every model time step, since N and Q are the prognostic variables in this two-moment bulk microphysical scheme. Thus, the hydrometeor mass distributions are always fully determined. The evolution of such a distribution is illustrated in Fig. 4.1, which depicts how the cloud droplet mass distribution shifts from larger masses to smaller masses during a MIMICA simulation due to a decrease in Q_c at constant N_c.

4.2 Ice habits

In contrast to the relatively uniform spherical geometry of liquid drops, ice crystals exhibit a vast diversity of shapes, referred to as habits (Fig. 4.2). The specific habit of an ice crystal is determined by the local thermodynamic

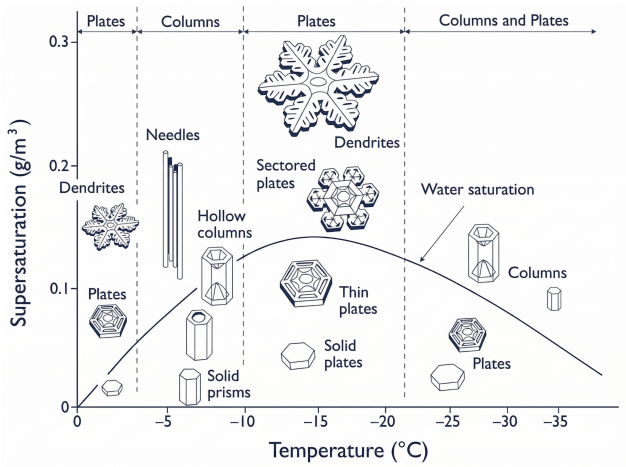

Figure 4.2: Ice crystal habits depending on temperature and ice supersaturation (Nakaya, 1954).
Image credit: Libbrecht (2019, modified)

conditions—primarily temperature and humidity—prevailing during its formation and subsequent growth. Consequently, the observed habit of an ice crystal provides a historical record of temperature and humidity conditions through which it has evolved. Complex three-dimensional ice crystals exist, but most crystals are characterized by two primary dimensions, such as length and width for columnar crystals, or diameter and thickness for plate-like crystals. Observational data have established robust relationships between these dimensions, leading to habit-specific mass-size relationships (Pruppacher and Klett, 2010). In the microphysical scheme of Seifert and Beheng (2006), this relationship is represented by a power law of the form:

$$D(m) = a \cdot m^b, \tag{4.4}$$

where D is the maximum diameter of the non-spherical hydrometeor, and the coefficients a and b depend on the habit. The geometric variations of the ice habit dictate the aerodynamic properties of the crystal, and thus the habit determines the terminal fall velocity (see Sect. 4.5.4).

Beyond influencing growth and sedimentation, the habit fundamentally controls how an ice crystal interacts with radiation. The non-spherical nature and varying surface complexity of different habits affect the scattering and absorption of light, posing a significant challenge for the remote sensing of ice-containing clouds. For instance, the backscattering of a radar signal is highly sensitive to the specific geometry and spatial orientation of the ice crystals. This complexity complicates retrievals, but the habit-dependent radiative signatures can also be exploited to identify the dominant ice habits within a cloud layer. To facilitate such analyses, numerous databases provide precalculated scattering properties for a wide variety of habits and size distributions (e.g., Hess and Wiegner, 1994; Eriksson et al., 2018).

4.3 Activation of cloud droplets

Condensation of water vapor requires the air to be supersaturated. However, for water droplets to form through homogeneous nucleation—without the presence of an assisting aerosol particle—supersaturations of approximately 500 % would be required (Lohmann et al., 2016). This high threshold exists because the energy gain from the phase transition is initially outweighed by the energetic cost of creating the surface between the liquid droplet and the surrounding air. As this surface-building cost increases for smaller radii, the saturation vapor pressure over a curved droplet surface is significantly higher than over a flat surface, an observation known as the Kelvin effect (dashed line in Fig. 4.3; Thomson, 1871). Hydrophilic[1] soluble aerosol particles facilitate droplet formation by serving as CCN. These particles adsorb water molecules and undergo hygroscopic growth below 100 % relative humidity, eventually dissolving to form a solution droplet. The presence of solute molecules lowers the equilibrium vapor pressure over the droplet surface according to Raoult's law (dash-dotted lines in Fig. 4.3; Raoult, 1886).

Köhler theory combines the Kelvin effect (enhanced saturation pressure over curved droplets) and Raoult's law (reduced saturation pressure over water solutions) to describe the heterogeneous formation of cloud droplets (solid lines in Fig. 4.3; Köhler, 1936). One form of the Köhler equation is given by Seinfeld and Pandis (2016):

$$\ln(S) = \ln\left(\frac{e_w(D)}{e^o}\right) = \frac{A}{D} - \frac{B}{D^3}, \tag{4.5}$$

where S is the saturation ratio, $e_w(D)$ is the saturation vapor pressure over a water droplet of diameter D, and e^o the saturation vapor pressure over a flat surface. The parameters A and B represent the Kelvin and Raoult terms, respectively, and are defined as:

$$A = \frac{4M_w\sigma_w}{RT\rho_w},\ B = \frac{6n_sM_w}{\pi\rho_w}, \tag{4.6}$$

with M_w being the molecular weight of water, σ_w the water surface tension, R the universal gas constant, T temperature, ρ_w the density of water, and n_s the number of moles of solute. For small droplets, the Raoult effect dominates, allowing the droplet to grow even in subsaturated conditions. As the droplet accumulates more water, the saturation vapor pressure over the solution droplet increases until it reaches a maximum value, known as the activation saturation ratio S_{act}, at the critical activation radius r_{act} (Fig. 4.3). Once the ambient supersaturation exceeds this critical threshold, the droplet overcomes the energy barrier and undergoes spontaneous, rapid growth. In summary, soluble aerosol particles act as CCN by significantly lowering the saturation ratio necessary for water vapor to condense into liquid droplets.

[1] Literally translated from Greek as "water-loving"; substance that easily interacts with water.

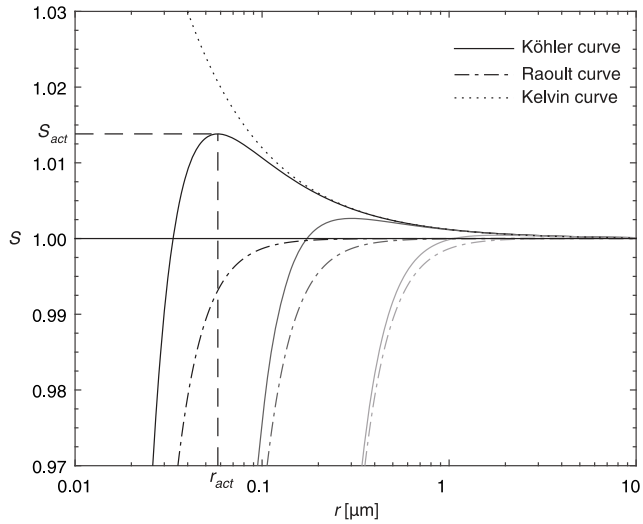

Figure 4.3: Köhler and Raoult curves for three NaCl aerosol particles with different dry radii (left to right: 0.01 µm, 0.03 µm and 0.1 µm). The Kelvin curve remains the same for all aerosol particles. S denotes the size-dependent saturation ratio of the solution droplet, see Eq. 4.5.
Image credit: Lohmann et al. (2016, modified). Reproduced with permission of Cambridge University Press through PLSclear.

4.4 Ice nucleation

Spontaneous freezing of supercooled liquid droplets in the atmosphere (homogeneous nucleation) occurs only at temperatures below approximately -38 °C. At higher temperatures, ice initiation requires the presence of ice-nucleating particles (INPs) to facilitate the phase change through heterogeneous nucleation. The various pathways through which atmospheric ice crystals form are categorized into several distinct modes:

- Homogeneous ice nucleation: the freezing of a cloud or solution droplet without the involvement of an INP.
- Immersion freezing: the initiation of freezing by an INP suspended within a supercooled cloud droplet at a temperature determined by the specific properties of the INP.
- Contact freezing: the immediate initiation of the phase change when an INP collides with the surface of a supercooled droplet.
- Deposition ice nucleation: the direct transition of water vapor to the solid phase on the surface of an INP.
- Condensation freezing: water vapor first condenses onto an INP at subzero temperatures and freezes immediately.

Observational studies of mixed-phase clouds consistently demonstrate that liquid cloud droplets generally form before ice nucleation is detected (e.g., Ansmann et al., 2009; de Boer et al., 2011; Westbrook and Illingworth, 2011). Consequently, immersion and contact freezing are considered the most relevant nucleation modes for these cloud types. The contribution of contact freezing is further constrained by the relatively low collision probability between supercooled droplets and interstitial, non-activated aerosol particles.

4.4.1 Heterogeneous ice nucleation

Similar to the activation of cloud droplets (Sect. 4.3), an energy barrier must be overcome for ice to form from supercooled liquid water. This barrier arises from the competition between the energy required to establish an interface between the supercooled water and the growing ice crystal, and the energetic gain associated with the phase transition from liquid to solid. Analogous to a CCN, an INP lowers this barrier by providing a surface that facilitates the attachment and phase alignment of water molecules (Whale, 2018).

Unlike the activation of cloud droplets, ice nucleation exhibits a strong dependence on temperature. However, laboratory experiments demonstrate that under constant thermodynamic conditions, the number of frozen droplets increases over time. These observations have led to two distinct conceptual frameworks for heterogeneous ice nucleation: the **deterministic** view and the **stochastic** view. The deterministic concept postulates that each individual INP possesses specific surface features, known as *active sites*, which trigger nucleation at a characteristic temperature or ice supersaturation. Under this assumption, the freezing efficiency varies between individual particles based on their surface characteristics. If an experiment is repeated with an identical set of droplets and INPs, the same droplets will freeze at exactly the same conditions as in the previous trial, implying that time has no impact on the frozen fraction. In contrast, the stochastic view assumes an inherent randomness to the nucleation process. In this framework, it is not possible to assign a specific activation threshold to an individual particle; instead, the probability of a nucleation event increases over time while temperature and saturation remain constant. Repeating an experiment with the same population of droplets results in a similar total frozen fraction, but the specific droplets that freeze will differ between iterations. According to a review of laboratory data, the surface characteristics and temperature dependence of INPs exert a much stronger influence on immersion freezing than time (Vali, 2014). This suggests that while the deterministic aspect of heterogeneous freezing dominates, the stochastic time dependence remains relevant under certain conditions. Heterogeneous freezing parameterizations adopt either of these assumptions. Deterministic schemes predict a set number of nucleation events based on aerosol surface area, size, or type (Phillips et al., 2008; DeMott et al., 2010; Niemand et al., 2012). Conversely, stochastic parameterizations use classical nucleation theory to calculate a nucleation rate based on particle characteristics (Hoose et al., 2010; Ickes et al., 2017).

4.4.2 Ice-nucleating particles

An aerosol particle must fulfill several physical criteria to function as an ice-nucleating particle (INP), including specific size requirements, insolubility, and particular crystallographic or chemical bond characteristics (Pruppacher and Klett, 2010). Likely, not all of these requirements must be met simultaneously; however, a solid surface appears to be a fundamental prerequisite for ice nucleation (Murray et al., 2012). Provided a solid surface is present, the specific efficiency of an INP depends heavily on the aerosol type; for instance, the crystallographic structure dictates the freezing characteristics of certain minerals, while specific surface proteins act as the critical active sites for biological aerosols. These specialized requirements restrict the number of potential INPs to approximately 1 in 10^5 aerosol particles (DeMott et al., 2010). Different aerosol types can act as INPs (Fig. 4.4): mineral dust particles are the most extensively investigated INPs, with laboratory reviews identifying them as primary drivers of nucleation at temperatures below approximately -15 °C (Hoose and Möhler, 2012). At higher temperatures, biological aerosol particles—such as bacteria, pollen, or fungal spores—are the primary initiators of ice nucleation. Additionally, the oceans serve as a significant source of INPs through the production of biogenic marine aerosol.

Measuring ambient INP concentrations

Ambient INP concentrations (INPCs) are primarily measured using two distinct methodologies. The first involves collecting aerosol particle samples on filters, which are subsequently immersed in a liquid to make the growth of ice crystals detectable (e.g., Bigg et al., 1963; Wex et al., 2019). The liquid suspension

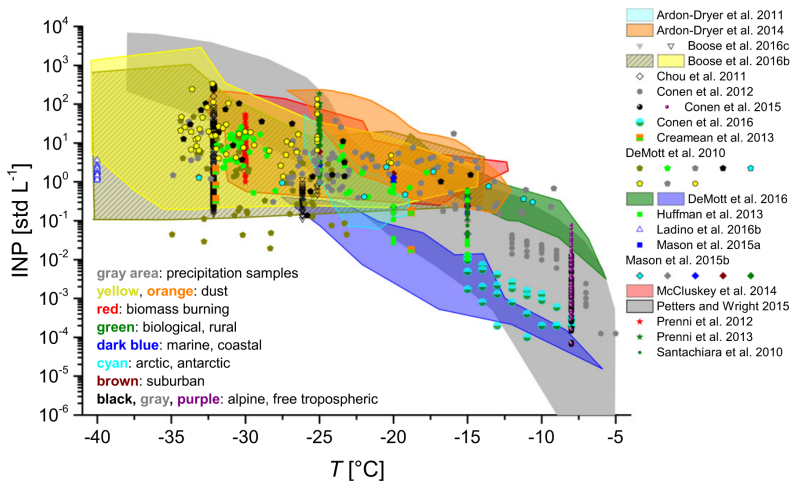

Figure 4.4: Compilation of INP observations.
Image credit: Kanji et al. (2017) © American Meteorological Society. Used with permission.

is then systematically cooled, allowing the number of freezing events to be recorded at specific temperatures. This offline method requires sampling large air volumes to collect a statistically significant number of INPs, resulting in a relatively coarse time resolution, often on the order of 24 h. Filter-based measurements are typically limited to temperatures above -25 °C, as unavoidable impurities in the liquid often trigger freezing below this threshold. The INPCs used in Paper 3 were obtained via this filter method using the Colorado State University (CSU) cold plate (e.g., Creamean et al., 2022). Direct observation of the experimental pipeline—from the initial suspension of particles from the filter and the subsequent dilution series to the final freezing trials in the cold plate—provided me with valuable insight into the rigorous laboratory work required to generate these datasets.

Alternatively, continuous flow diffusion chambers (CFDCs) allow for the in-situ analysis of ambient INPCs (e.g., Rogers, 1988; Garimella et al., 2016). In these instruments, a continuous air stream passes through a chamber with ice-covered walls that are heated differentially to create a specific temperature and supersaturation. Ice crystals that grow on the INPs within the flow are then detected optically. To prevent the misidentification of liquid droplets as ice, the flow enters an evaporation section maintained at ice saturation prior to detection. Depending on the specific instrument setup, CFDCs can typically cover a temperature range from -15 to -50 °C. Their sensitivity is limited by the optical detection threshold and the inherent effectiveness of the sampled INP population.

The characteristic distribution of INP concentrations

Fig. 4.4 shows the cumulative INP concentration depending on temperature. Cumulative INP concentrations exhibit a clear exponential dependence on temperature. This exponential dependence reflects the strong temperature sensitivity of nucleation rates predicted by classical nucleation theory (Pruppacher and Klett, 2010).

When examining the relative distribution of ambient INPCs at a fixed temperature, the population often follows a log-normal distribution (e.g., Isaac and Douglas, 1971; Welti et al., 2018). Such a distribution suggests that the INP population has undergone significant dilution during atmospheric transport, indicating that the primary sources are likely distant from the measurement site (Ott, 1990). The characteristic log-normal distribution of INPCs at a specific temperature provided the physical basis for the ice nucleation parameterization formulated in Paper 1.

4.4.3 Prescribed ice crystal number concentration

Numerical models using prognostic ice nucleation schemes frequently struggle to simulate sufficient ice mass in MPCs, particularly at higher temperatures where INPs are scarce. To circumvent this limitation, models often prescribe ice crystal number concentrations (ICNC; e.g., Savre et al., 2014; Loewe et al., 2017; Stevens et al., 2018), an approach we implemented in Paper 3. Under

specific thermodynamic and microphysical conditions—such as falling below a temperature threshold or exceeding a minimum cloud droplet mass—a specified ICNC (ICNC_0) is enforced by freezing as many existing cloud droplets as necessary. For example, in Paper 3, the change in ICNC (ΔICNC) in grid cells where $T < -5$ °C and $Q_c \geq 10^{-7}\,\mathrm{kg\,kg^{-1}}$ was calculated as:

$$\Delta\mathrm{ICNC} = \max\left[\min(N_c, \mathrm{ICNC}_0) - \mathrm{ICNC}, 0\right]. \tag{4.7}$$

This setup decouples the ice phase from heterogeneous nucleation pathways. By forcing the model to maintain a predefined number of ice crystals, the broader microphysical impacts of the ice can be isolated without relying on uncertain relationships between INPs and the final ICNC. However, the definition of a realistic ICNC_0 introduces a new uncertainty, which Paper 3 explores.

4.5 Growth and sinks of hydrometeors

Newly formed cloud droplets and ice crystals are small enough to remain suspended by in-cloud updrafts. To overcome these updrafts and fall as precipitation, the hydrometeors must undergo significant growth. For comparison, a typical cloud droplet has a diameter of approximately 10 μm, while a typical raindrop has a diameter of 2 mm. Consequently, the mass of a cloud droplet must increase by approximately seven orders of magnitude to become a raindrop capable of falling toward the surface.

4.5.1 Diffusional growth, evaporation and sublimation

Once liquid droplets reach the activation radius (Sect. 4.3), they grow spontaneously via the diffusion and condensation of water vapor, provided the environment remains supersaturated. The same principle applies to ice crystals, if the ambient vapor pressure exceeds the saturation pressure with respect to ice. Conversely, if the vapor pressure falls below the saturation pressure of the respective phase, liquid droplets begin to evaporate and ice crystals begin to sublimate. The change in mass of a ventilated droplet—which moves relative to its surrounding air—due to condensation or evaporation is expressed as (Pruppacher and Klett, 2010):

$$\frac{dm}{dt} = 2\pi D D_v \bar{f}_v \left(\rho_{v,\infty} - \rho_v(D)\right), \tag{4.8}$$

where D_v is the diffusivity of water vapor in air, $\bar{f}_v$ is the mean ventilation coefficient for vapor diffusion, $\rho_{v,\infty}$ is the bulk density of water vapor, and $\rho_v(D)$ is the density of water vapor at the surface of the droplet. The change in mass of a ventilated ice crystal due to deposition or sublimation is similarly defined as:

$$\frac{dm}{dt} = 2\pi D_v C \bar{f}_v(\rho_{v,\infty} - \rho_{v,s}), \tag{4.9}$$

with C the capacitance, which accounts for the specific ice crystal habit, and $\rho_{v,s}$ the density of water vapor at the surface of the ice crystal.

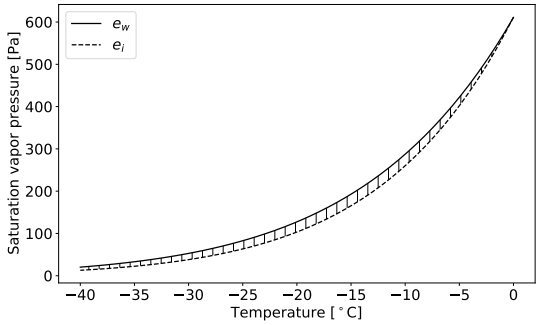

Figure 4.5: Saturation pressures over water (e_w, solid) and ice (e_i, dashed). Between the saturation pressures, the WBF process is active (shaded).

A fundamental aspect of cloud microphysics is that the saturation pressure over water is always higher than over ice (Fig. 4.5). When liquid and frozen hydrometeors coexist at a vapor pressure between saturation over water and ice, the frozen hydrometeors grow at the expense of evaporating liquid droplets. This mechanism is known as the Wegener-Bergeron-Findeisen process (WBF process; Wegener, 1911; Bergeron, 1935; Findeisen, 1938). The efficiency of the WBF process explains why Paper 3 identifies the ice habit as a primary determinant of whether the simulated cloud glaciates or not.

4.5.2 Collection processes

Diffusional growth alone cannot produce precipitation-sized hydrometeors within relevant atmospheric time spans. The collision and collection of diverse hydrometeors provide a significantly more efficient growth pathway. These processes reach maximum efficiency when hydrometeors exhibit substantial size differences—leading to varying fall velocities that increase collision probability—and when cloud turbulence introduces additional relative velocity components.

The following collection processes occur in mixed-phase clouds:

- Collision-coalescence: liquid droplets collide and merge to form a larger liquid droplet.
- Aggregation: ice crystals collide and stick together to form an ice crystal aggregate.
- Riming: liquid droplets collide with a frozen hydrometeor and freeze on its surface, forming graupel or hail.

A collision between two hydrometeors does not automatically lead to the formation of a single, larger hydrometeor. The outcome depends on the coalescence efficiency for liquid droplets, or sticking efficiency for ice crystals; without a sufficiently high efficiency, the hydrometeors may simply rebound and separate.

Mathematically, the stochastic collection equation (SCE; Berry, 1967) describes collisions between hydrometeors with mass distribution functions $f(m_x - m_y)$ and $f(m_y)$:

$$\begin{aligned}\frac{\partial f(m_x)}{\partial t} = &\frac{1}{2}\int_0^{m_x} f(m_x - m_y) f(m_y) K(m_x - m_y, m_y) dm_y \\ &- \int_0^{\infty} f(m_x) f(m_y) K(m_x, m_y) dm_y.\end{aligned} \tag{4.10}$$

The first term represents all collisions forming a droplet of mass m_x, while the second term accounts for the sink of droplets of mass m_x due to collisions with other droplets. The collection kernel, K, defines the encounter probability based on geometric cross-sections, relative fall velocities, and the collision efficiency of the interacting hydrometeors.

Over continental regions, approximately 95 % of the rain originates from clouds containing ice (Mülmenstädt et al., 2015). Given this dominance of the ice phase, collection processes involving frozen hydrometeors—specifically riming and aggregation—act as the fundamental drivers of terrestrial precipitation, highlighting the critical role of cloud phase.

4.5.3 Melting

When the temperature rises above 0 °C, ice crystals and snowflakes begin to melt. The phase transition itself does not immediately alter the total mass of the hydrometeor, yet it fundamentally changes other physical properties. Specifically, the new phase dictates the interaction of the hydrometeor with radiation and the probability of it colliding and sticking to other hydrometeors (Sect. 4.5.2). Furthermore, it is important to note that the higher saturation vapor pressure of water compared to ice makes evaporation more likely to occur from liquid than from frozen hydrometeors.

The rate at which the ice mass, m_i, within a spherical hydrometeor converts to liquid water can be calculated according to Pruppacher and Klett (2010):

$$\frac{dm_i}{dt} = -\frac{2\pi D}{L_m}\left(k_a(T - T_0)\bar{f}_h + \frac{D_v L_e M_w}{R}\left[\frac{e}{T} - \frac{e_r}{T_0}\right]\bar{f}_v\right). \tag{4.11}$$

Here, L_m represents the latent heat for melting of ice, k_a is the heat conductivity of air, $T_0 = 273.15\,\mathrm{K}$, $\bar{f}_h$ is the mean ventilation coefficient for heat diffusion, L_e is the latent heat of evaporation of water, M_w is the molecular weight of water, e is the partial pressure of water vapor in air, and e_D is the partial pressure of water vapor over a spherically curved water surface.

4.5.4 Precipitation

The most efficient sink for a cloud is the physical removal of hydrometeors via precipitation. Hydrometeors descend toward the surface once they attain sufficient mass for their fall velocity to overcome the cloud updrafts. If the air below the cloud is significantly subsaturated, the hydrometeor may evaporate or

sublimate entirely before reaching the surface, which redistributes moisture to lower altitudes. Similarly, falling frozen hydrometeors may melt when traversing air layers above the freezing point, often reaching the surface as rain instead of snow.

The hydrometeor fall speed v is described by a power-law relationship with mass (Seifert and Beheng, 2006):

$$v(m) = \alpha \cdot m^{\beta} \left(\frac{\rho_0}{\rho} \right)^{\gamma}, \tag{4.12}$$

where the coefficients α, β, and γ depend on the hydrometeor type; for ice crystals, these values specifically depend on the ice habit. The variables ρ_0 and ρ represent the air density at the surface and at the specific altitude, respectively. The density correction term accounts for the reduction in aerodynamic drag as hydrometeors descend through the atmosphere.

4.6 Secondary ice processes

Observations of ice crystal number concentrations in clouds warmer than -38 °C often exceed INP concentrations by several orders of magnitude (e.g., Hobbs and Rangno, 1985; Pasquier et al., 2022). Several mechanisms have been described that enhance the ice crystal number without requiring primary ice nucleation, so-called secondary ice processes (SIPs). The following sections discuss the most prominent of these processes.

Collisional breakup

This mechanism occurs when collisions between frozen hydrometeors cause fragments to splinter from either of the colliding hydrometeors (see Fig. 4.6a; e.g., Vardiman, 1978). Models frequently parameterize this process following Phillips et al. (2017b), who define the number of fragments produced per

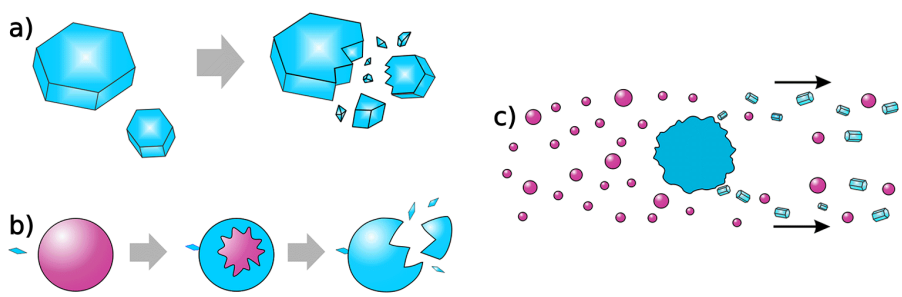

Figure 4.6: SIP processes a) collisional breakup, b) drop shattering, and c) rime splintering. Liquid phase in magenta colors, ice phase in blue colors. Image credit: Korolev and Leisner (2020, modified)

collision, F_{BR}, as:

$$F_{BR} = \alpha_h A \left(1 - \exp\left\{-\left[\frac{C_A K_0}{\alpha_h A}\right]_r^{\gamma}\right\}\right). \tag{4.13}$$

Here, α_h is the equivalent-spherical surface area of the smaller, fracturing hydrometeor; A is the number density of asperities susceptible to breaking and depends on the hydrometeor type, size, rimed fraction, and the temperature; C_A is the asperity-fragility coefficient and also depends on the hydrometeor type; γ_r is a function of the rimed fraction and hydrometeor type; and K_0 is the collisional kinetic energy driving the fragmentation:

$$K_0 = 0.5 \frac{m_1 m_2}{m_1 + m_2} (v_1 - v_2)^2, \tag{4.14}$$

with m_1, m_2 the masses of the two colliding hydrometeors, and v_1, v_2 their respective fall velocities. This parameterization is valid for any frozen hydrometeors with diameters ranging from 0.5 to 5 mm.

Drop shattering

As a supercooled droplet freezes from its outermost layer inward, internal pressure accumulates within the droplet (e.g., Lauber et al., 2018). This pressure buildup can lead to the shattering of the droplet and its newly formed ice shell, which ejects small ice fragments (Fig. 4.6b). Phillips et al. (2018) proposed two distinct modes for this process: mode 1 describes shattering following a collision with a smaller ice crystal—where the mass of the ice crystal is smaller than the mass of the drop—or during heterogeneous freezing, while mode 2 characterizes shattering after a collision with a larger frozen hydrometeor. Mode 1 produces F_{DS_1} fragments defined as:

$$F_{DS_1} = \Xi(D_r)\Omega(T) \left[\frac{\zeta \eta^2}{(T - T_0)^2 + \eta^2} + \phi T\right], \tag{4.15}$$

where D_r is the diameter of the raindrop, the cubic interpolation functions $\Xi(D_r)$ and $\Omega(T)$ limit the scheme to $D_r \geq 0.05$ mm and $T \leq$ -3 °C, while ζ, η, and ϕ are additional coefficients depending on D_r. Mode 2 produces F_{DS_2} fragments resulting from the collision of a drop with a frozen hydrometeor of greater mass:

$$F_{DS_2} = 3\Phi(T)\left[1 - f_{DS_2}(T)\right] \times \max(\mathrm{DE} - \mathrm{DE}_{crit}, 0). \tag{4.16}$$

Here, $\Phi(T)$ represents the empirical probability that a produced secondary droplet contains ice, $f_{DS_2}(T)$ describes the fraction of droplets already frozen initially due to supercooling, $\mathrm{DE} = \frac{K_0}{\sigma_w \pi D_r^2}$ is the dimensionless energy with DE_{crit} defining the threshold for the onset of splashing upon collision.

Rime splintering

This mechanism, frequently referred to as Hallett-Mossop process (Hallett and Mossop, 1974) occurs during the riming of supercooled droplets onto

larger frozen hydrometeors, such as snowflakes, graupel or large frozen drops (Fig. 4.6c). As with drop shattering, the accumulation of internal pressure during the freezing of the accreted liquid leads to the ejection of secondary ice splinters. Observations indicate that this process remains active specifically at temperatures between -8 and -3 °C. Reisner et al. (1998) formulated this process mathematically as:

$$F_{RS} = 3.5 \times 10^8 \rho \, f_{RS}(T) \, m_{rime}, \tag{4.17}$$

with $f_{RS}(T)$ restricting the formulation to $265\,\mathrm{K} \leq T \leq 270\,\mathrm{K}$, and m_{rime} the mass of rime accumulated on the frozen hydrometeor.

By including these secondary mechanisms, numerical models can better bridge the gap between primary ice nucleation and the high ice crystal concentrations observed in natural clouds (e.g., Phillips et al., 2017a; Sullivan et al., 2018; Sotiropoulou et al., 2020).

4.7 Net effects of microphysics

To determine the evolution of a cloud system, the individual processes described in this chapter must be integrated over the size distributions of all hydrometeor classes. This integration yields the net change in the bulk number concentrations (N) and mixing ratios (Q). The resulting total changes, dN and dQ, account for the competition between various sources and sinks. For simplicity, the following equations define these tendencies specifically for cloud droplets (subscript c) and ice crystals (subscript i):

$$\begin{aligned}
dN_c &= dN_{c,act} - dN_{c,freez} - dN_{c,coll} \\
dQ_c &= dQ_{c,act} + dQ_{c,cond} - dQ_{c,freez} - dQ_{c,evap} - dQ_{c,coll} \\
dN_i &= dN_{i,freez} + dN_{i,SIP} - dN_{i,coll} - dN_{i,melt} - dN_{i,precip} \\
dQ_i &= dQ_{i,freez} + dQ_{i,dep} + dQ_{i,SIP} - dQ_{i,subl} - dQ_{i,coll} \\
&\quad - dQ_{i,melt} - dQ_{i,precip}.
\end{aligned} \tag{4.18}$$

Table 4.1 defines the abbreviations for each microphysical process. Note that the freezing terms are coupled, such that $dN_{c,freez} = dN_{i,freez}$ and $dQ_{c,freez} = dQ_{i,freez}$, representing the direct transfer of mass and number between the liquid and ice phases.

The microphysical representations in the version of MIMICA used in Paper 3 follow the formulations described throughout this chapter. In contrast, Paper 1 applied an earlier version of MIMICA; in that configuration, the microphysics involving frozen hydrometeors followed the parameterizations of Wang and Chang (1993) rather than those of Seifert and Beheng (2006). The climate models analyzed in Paper 2 employ diverse stratiform microphysics schemes: two of these models use two-moment schemes, while one employs a one-moment scheme that prognoses only the mass mixing ratio of hydrometeors. Common to all these numerical frameworks is the coupling between microphysical processes

Table 4.1: Abbreviations for microphysical processes listed in Eq. 4.18.

Abbreviation	Process
act	Activation of cloud droplets
freez	Freezing of cloud droplets to ice crystals
coll	Collision
cond	Condensation of water vapor
evap	Evaporation of liquid droplets
SIP	Secondary ice processes
melt	Melting of ice crystals (which in MIMICA only produces raindrops, no cloud droplets)
precip	Precipitation (which does not affect cloud droplets in MIMICA because they are assumed to have no fall velocity)
dep	Deposition of water vapor
subl	Sublimation from frozen hydrometeors

and the larger-scale dynamics. Within this coupled system, hydrometeor masses undergo advection and influence the atmospheric flow, while the exchange of latent heat directly modifies the modeled potential temperature.

Chapter 5

Summary of appended papers and outlook

This thesis addresses the representation of cloud phase in mixed-phase clouds (MPC) and aims at advancing the modeling of these clouds. To this end, three studies were conducted using both LES (large-eddy simulation) and GCM (general circulation model) frameworks. The first study proposes a new ice nucleation parameterization, the second evaluates the relative importance of four microphysical processes across three different GCMs, and the final study investigates the sensitivity of an Arctic MPC to aerosol and microphysical quantities.

5.1 An ice nucleation parameterization incorporating stochastic variability

Accurately modeling both the liquid and ice phase is essential to represent clouds and their radiative interactions, as well as precipitation formation. A primary driver of cloud phase is heterogeneous ice nucleation, a process occurring at scales so small that it always must be parameterized in atmospheric models. However, the parameterization of heterogeneous ice nucleation typically suffers from three common drawbacks:

- Computational complexity: These schemes often require detailed input from the driving model, such as aerosol number concentrations, type and/or size. The availability of this input depends on the specific model and the aerosol particle species implemented within it. This input requirement creates a significant constraint, as parameterizations based on observations of very specific aerosol types, such as fungal spores or bacteria, are incompatible with models that lack a detailed differentiation between aerosol particle species.
- Limited validity: These parameterizations can be restricted to specific

ranges of temperature or vapor saturation, depending on the underlying measurements.

- Lack of INPC (ice-nucleating particle concentration) variability: Most schemes yield a single, fixed INPC value for a given set of conditions (temperature, vapor saturation, aerosol concentration, aerosol particle size and type). This static value serves as the base for the ice nucleation parameterization. Such a static approach fails to represent the full range and variability of observed values.

Paper 1 addresses all of these limitations by introducing a stochastic approach: The scheme only requires temperature as input from the driving model and remains valid across the entire temperature range of heterogeneous freezing. By drawing INPC values randomly from a relative frequency distribution (RFD), the parameterization returns an INPC that reflects the full range and variability of observations. This INPC RFD is derived from the observations that INPCs at a given temperature follow a log-normal frequency distribution. The resulting RFD is valid for remote locations.

The Arctic is representative of such pristine conditions, and thus we tested the new parameterization in a large-eddy simulation (LES) of a relatively warm AMPS (Arctic mixed-phase stratiform cloud) with in-cloud temperatures between -7 and -10 °C using the MIMICA model. LES modeling of AMPS provides an ideal testbed for new microphysical parameterizations due to the typical longevity of these clouds and their high sensitivity to cloud phase. The ice content of the resulting simulated cloud exhibited a magnitude consistent with observations. The results showed that cloud ice content depends linearly on the median INPC of the RFD, and exponentially on the standard deviation of the distribution. A sensitivity test with a fixed median INPC instead of random drawing from the RFD resulted in almost no cloud ice. This result highlights the importance of the stochastic approach, as the consistent application of a single value is equivalent to standard parameterizations that yield only one INPC value for a given set of input parameters. However, the amount of cloud ice was also sensitive to the frequency of the random draws and the model resolution. Essentially, a reduction in the total number of draws—resulting from either a lower drawing frequency or coarser spatial resolution with fewer grid cells—led to a corresponding decrease in the modeled IWP. This dependency presents a significant challenge for the implementation of the scheme into different models, particularly those operating with lower temporal or spatial resolution. Nevertheless, this work demonstrates that a parameterization based on random drawing from an INPC RFD can improve the LES of AMPS, although further amendments are still required (see Outlook). Following these refinements, our heterogeneous ice nucleation parameterization will allow for straightforward implementation into global models. Once properly tuned, such an integration has the potential to enhance the global representation of cloud phase.

5.2 Divergent cloud phase sensitivity to microphysical processes across global climate models

The relative importance of ice nucleation compared to three other microphysical processes that directly affect the amount of ice in MPCs is analyzed in Paper 2. Additionally, the spatial resolution coarsens from LES to the global scale, since three general circulation models (GCMs) are compared. We applied a factorial analysis to determine the impact of primary ice nucleation (PIN), secondary ice production (SIP), sedimentation, and transport of ice crystals. The objective was to identify whether the models agree that certain processes dominate, which would allow for targeted recommendations on where to focus model development. However, the three models converge only in one specific area: PIN dominates in high northern latitudes at low mixed-phase temperatures. In all other mixed-phase temperature ranges and regions, the models fail to reach a consensus on the most or least important process.

We additionally implemented a unified SIP parameterization across the three GCMs to compare one specific process in a consistent framework. Despite this identical representation, the importance of SIP varied substantially between the models. One model showed no response to SIP regarding the cloud phase, while the other two exhibited varying sensitivities across temperatures and geographical locations. This result demonstrates that fundamental differences exist in how microphysical processes interact with the rest of each model framework.

Together with the process analysis, the main implication of our findings is that microphysical process studies based on single models cannot claim general results for the global climate system. Furthermore, the divergence in the relative importance of the four processes suggests that it is preferable to obtain direct process rates from observations rather than relying on state variables to tune model processes. Additionally, we conclude that microphysical processes must be viewed as a collective, both in terms of observational constraints and model representation. Finally, this work questions whether the traditional approach of treating cloud microphysics as a chain of individual processes remains appropriate, or if it is instead possible to describe microphysics as a single net process.

5.3 Cloud-phase sensitivities to aerosol and microphysical parameters

Paper 3 shifts focus from microphysical processes to individual observables that are input into models, analyzing which out of four parameters exert the greatest influence on the cloud phase of a separate AMPS.

The original objective of this study was to combine vertically resolved aerosol particle and INP observations into a closure study using the MIMICA LES model. However, an ice nucleation parameterization based on observed

in-cloud INP concentrations resulted in no simulated cloud ice because the INP concentrations were too low. Consequently, it was necessary to prescribe ICNC (ice crystal number concentration) to reproduce the observed LWP (liquid water path) and IWP (ice water path).

We transitioned to a factorial analysis to evaluate how simulated LWP, IWP, and downward longwave radiation at the surface (DWLW) respond to variations in aerosol number concentration (ANC), aerosol type, ICNC, and ice habit. Using two values per parameter, this approach revealed that ANC had the largest impact on simulated LWP and DWLW. This high sensitivity originates from the lower ANC value reaching the CCN-limited regime, where concentrations are too low to provide sufficient CCN for the condensation of all available water vapor, even at saturated conditions (Mauritsen et al., 2011). These results suggest that ANC must be measured at cloud level rather than the surface to remain representative, as discrepancies between surface measurements and in-cloud droplet numbers occurred in this specific case (Pohorsky et al., 2026). ICNC clearly dominated the variability of IWP, and was the second-most important parameter for LWP and DWLW. This parameter impacts the simulated cloud phase directly, as it prescribes the minimum number of ice crystals in cloud regions where the temperature is below -5 °C, and the two tested ICNC values differ by two orders of magnitude. Ice habit consistently ranked third among the four parameters, yet it dictated whether the cloud remained mixed-phase or transitioned into a purely liquid or ice state. The two tested ice habits in this study are columns and plates; for a given mass, plates exhibit a larger characteristic size in MIMICA, which leads to enhanced deposition. In cases with high ICNC, this increased deposition triggered total cloud glaciation via the WBF (Wegener-Bergeron-Findeisen) process, showing that the influence of habit remains closely coupled to ICNC. In contrast, aerosol type exerted only a negligible influence on this specific case.

This study demonstrates that the overall phase state of AMPS can be crucially determined by the ice habit, highlighting that models need to distinguish between different ice habits. We conclude that observing ANC, ICNC (or INP concentrations up to warm temperatures alongside secondary ice processes), and ice habit is essential for future Arctic campaigns. To be most relevant for modeling, these properties should be observed at cloud level rather than at the surface. Successful integration of such observations requires models to possess the specific capability to process this information, particularly the ice habit.

5.4 Concluding remarks and outlook

Motivated by the critical role of cloud phase in cloud-radiation interactions and precipitation formation, this thesis aimed to advance the modeling of cloud phase in MPCs. Drawing upon both LES and GCM frameworks, the primary conclusions are summarized as follows:

- This work developed a new heterogeneous ice nucleation parameterization that generates significant ice mass in a relatively warm AMPS. The

scheme incorporates random drawing from INP concentration distributions based on observations, thereby overcoming typical limitations of other parameterizations.

- A comparison across three GCMs demonstrated a lack of consensus regarding the relative importance of four microphysical processes, indicating that single-model studies cannot definitively characterize process importance in the global climate system. The divergence among models questions whether the traditional approach of representing individual microphysical processes in isolation remains appropriate for large-scale model frameworks.

- Large-eddy simulations of a different relatively warm AMPS revealed that cloud phase is highly sensitive to ANC, ICNC and ice habit, whereas aerosol type exerts negligible influence. These findings specify crucial observational targets in future Arctic campaigns and highlight the need for habit-sensitive microphysical parameterizations.

This research provides direct suggestions for model improvement and simultaneously identifies new questions for future investigations. The following sections describe potential research projects designed to further advance the modeling of mixed-phase clouds.

5.4.1 Refining and scaling the stochastic freezing parameterization in Paper 1

A primary step following Paper 1 is to further investigate the frequency of random drawing and the impact of model resolution, as both factors likely influence the portability of the scheme to other models. In the current implementation, a random selection occurs for each model grid cell at every time step; consequently, the degree of randomness depends on the model resolution. To resolve this dependency, the spatial and temporal variability of the random drawing could be constrained independently of the model grid scale. Alternatively, for coarse-resolution models, sub-stepping within each grid box could be performed by drawing more frequently than the actual model time step.

Following the mitigation of these resolution dependencies, the next natural step involves evaluating the parameterization within different models and across a wider variety of cloud cases. Specifically, testing the scheme for cases with lower temperatures is essential, as these conditions exhibit significantly higher rates of ice nucleation. Ideally, such cases would include reliable observations of cloud ice to enable a more quantitative evaluation of the parameterization. Apart from varying thermodynamic conditions, diverse aerosol populations and sources should also be investigated. The INPC distributions must be adapted for such cases, as the current formulation assumes remote maritime aerosol particles. This adaptation can be achieved by modifying the median and width of the INPC RFD to the new aerosol population. Applying the scheme to diverse cases and models would provide deeper insights into its universality.

5.4.2 Regional GCM analysis and comparison with the SOCRATES campaign

A follow-up study to Paper 2 is currently in progress, using GCM simulations restricted to the Southern Ocean with increased temporal resolution: the analysis in Paper 2 was based on monthly averages, while the Southern Ocean study will be based on three-hourly values. During the simulated period, the extensive SOCRATES aircraft campaign (McFarquhar et al., 2021) provided comprehensive in-situ and remote sensing observations of the vertical distributions of clouds and aerosol particles, including CCN and INPs. The primary objective of this study is to perform a factorial analysis to quantify process relevance on this smaller domain while leveraging the vast observational data to evaluate model performance of all three models. The Southern Ocean remains a region where most GCMs exhibit their largest radiation biases; consequently, we anticipate that the models will again lack consensus regarding the relative importance of the four microphysical processes. However, the high-quality observations from SOCRATES may permit process-based evaluations that can be compared directly with the GCM simulations. By moving from monthly and large-scale averages to a data-rich regional focus, we aim to identify whether the inter-model divergence stems from fundamental differences in process interactions or from the misrepresentation of specific aerosol-cloud environments.

5.4.3 Expanding the parameter space and ice habit dependencies in Paper 3

Broadening the parameter space of Paper 3 would provide valuable physical insights. One promising approach involves replacing the prescribed ICNC with an evaluation of two different ice nucleation parameterizations. Possible schemes to include are the one proposed in Paper 1 and the parameterization by DeMott et al. (2010) which depends on temperature and the concentration of large aerosol particles. The latter option is particularly feasible, as vertical concentration measurements for large aerosols are available from the analyzed campaign. Transitioning from a prescribed ICNC to prognostic ice nucleation schemes would establish a more physically rigorous simulation setup. Furthermore, employing a scheme that depends on the entire aerosol size distribution (e.g., Phillips et al., 2008) could lead to a stronger influence of ANC on IWP.

Investigating specific habit-dependent coefficients within MIMICA offers a second logical extension. Our findings in Paper 3 indicated that the mass-size relationship primarily influences the simulated cloud via the deposition rate. However, other coefficients in the deposition rate equation and the mass-fall velocity relationship also depend on the ice habit and may exert a considerable impact. Isolating the individual contributions of these various factors would further clarify the physical mechanisms through which ice habit governs cloud evolution.

Expanding the factorial analysis to include turbulence and boundary conditions represents a third pathway. Potential MIMICA input variables include surface roughness lengths, the turbulent Prandtl number, surface temperature,

geostrophic wind, or large-scale divergence. Combining some of these parameters with the previous aerosol and microphysical parameters could clarify whether cloud microphysics, turbulence, or boundary conditions exert the dominant influence on the simulated AMPS.

5.4.4 Implementing a radar simulator into MIMICA

During the investigation of the AMPS case in Paper 3, I began comparing the MIMICA simulations against additional cloud radar observations. Specifically, radar reflectivity and the radar-derived Doppler velocity of hydrometeors are, in theory, relatively straightforward to calculate in MIMICA. For specific hydrometeor sizes and shapes, the radar reflectivity is proportional to the second moment of the mass distribution. However, the non-spherical shape of ice crystals can cause significant discrepancies when calculations rely solely on mass distribution. To address this, one group in our division at Chalmers has developed an extensive database of scattering properties for various ice habits, spanning diverse size distributions and instrument frequencies. A logical continuation of this initiated work would be to fully incorporate habit-dependent calculations of radar reflectivity and Doppler velocity into MIMICA. This integration would permit a more robust comparison between simulations and observations, moving beyond integrated bulk properties like LWP and IWP to include more direct cloud radar measurements.

Furthermore, a co-author of Paper 3 has already initiated related work to retrieve cloud-top ICNC from radar data. This retrieval process relies on several assumptions regarding the ice crystal size distribution and the parameters of the ice crystal size-fall velocity relationship. Comparing these variables—ICNC, size distribution parameters, and size-fall velocity relationship parameters—with MIMICA simulations will provide a critical evaluation of MIMICA simulations and the assumptions currently used within the model.

List of Figures

Bibliography

Ansmann, A., M. Tesche, P. Seifert, D. Althausen, R. Engelmann, J. Fruntke, U. Wandinger, I. Mattis and D. Müller (2009). "Evolution of the Ice Phase in Tropical Altocumulus: SAMUM Lidar Observations over Cape Verde". In: *J. Geophys. Res. Atmospheres* 114.D17. ISSN: 2156-2202. DOI: 10.1029/2008JD011659.

Arakawa, A. (2004). "The Cumulus Parameterization Problem: Past, Present, and Future". In: *J. Clim.* 17.13, pp. 2493–2525. ISSN: 0894-8755, 1520-0442. DOI: 10.1175/1520-0442(2004)017<2493:RATCPP>2.0.CO;2.

Arouf, A., H. Chepfer, J. E. Kay, T. S. L'Ecuyer and J. Lac (2024). "Surface Cloud Warming Increases as Late Fall Arctic Sea Ice Cover Decreases". In: *Geophys. Res. Lett.* 51.3, e2023GL105805. ISSN: 1944-8007. DOI: 10.1029/2023GL105805.

Bardakov, R., I. Riipinen, R. Krejci, J. Savre, J. A. Thornton and A. M. L. Ekman (2020). "A Novel Framework to Study Trace Gas Transport in Deep Convective Clouds". In: *Journal of Advances in Modeling Earth Systems* 12.5. e2019MS001931 10.1029/2019MS001931. DOI: https://doi.org/10.1029/2019MS001931. eprint: https://agupubs.onlinelibrary.wiley.com/doi/pdf/10.1029/2019MS001931.

Bergeron, T. (1935). "On the physics of clouds and precipitation". In: Proc. Fifth Assembly of the International Union of Geodesy and Geophysics. International Union of Geodesy and Geophysics. Lisbon, Portugal, pp. 156–180.

Berry, E. X. (1967). "Cloud Droplet Growth by Collection". In: *J. Atmospheric Sci.* 24.6, pp. 688–701. ISSN: 0022-4928, 1520-0469. DOI: 10.1175/1520-0469(1967)024<0688:CDGBC>2.0.CO;2.

Bigg, E. K., S. C. Mossop, R. T. Meade and N. S. C. Thorndike (1963). "The Measurement of Ice Nucleus Concentrations by Means of Millipore Filters". In: *J. Appl. Meteorol. Climatol.* 2.2, pp. 266–269. ISSN: 1520-0450. DOI: 10.1175/1520-0450(1963)002<0266:TMOINC>2.0.CO;2.

Birch, C. E., I. M. Brooks, M. Tjernström, M. D. Shupe, T. Mauritsen, J. Sedlar, A. P. Lock, P. Earnshaw, P. O. G. Persson, S. F. Milton and C. Leck (2012). "Modelling Atmospheric Structure, Cloud and Their Response to CCN in the Central Arctic: ASCOS Case Studies". In: *Atmos. Chem. Phys.* 12.7, pp. 3419–3435. ISSN: 1680-7324. DOI: 10.5194/acp-12-3419-2012.

Boucher, O., S. Denvil, G. Levavasseur, A. Caubel, A. Cozic, M.-A. Foujols, Y. Meurdesoif, P. Cadule, M. Devilliers, J. Ghattas, N. Lebas, T. Lurton, L.

Mellul, I. Musat, J. Mignot and F. Cheruy (2023). *IPSL IPSL-CM6A-MR1 model output prepared for CMIP6 CMIP*. DOI: 10.22033/ESGF/CMIP6.15922.

Brooks, I. M., M. Tjernström, P. O. G. Persson, M. D. Shupe, R. A. Atkinson, G. Canut, C. E. Birch, T. Mauritsen, J. Sedlar and B. J. Brooks (2017). "The Turbulent Structure of the Arctic Summer Boundary Layer During The Arctic Summer Cloud-Ocean Study". In: *J. Geophys. Res. Atmospheres* 122.18, pp. 9685–9704. ISSN: 2169-8996. DOI: 10.1002/2017JD027234.

Bryan, G. H. and J. M. Fritsch (2002). "A benchmark simulation for moist nonhydrostatic numerical models". In: *Monthly Weather Review* 130, pp. 2917–2928.

Bulatovic, I., A. M. L. Ekman, J. Savre, I. Riipinen and C. Leck (2019). "Aerosol Indirect Effects in Marine Stratocumulus: The Importance of Explicitly Predicting Cloud Droplet Activation". In: *Geophys. Res. Lett.* 46.6, pp. 3473–3481. ISSN: 1944-8007. DOI: 10.1029/2018GL081746.

Bulatovic, I., J. Savre, M. Tjernström, C. Leck and A. M. L. Ekman (2023). "Large-Eddy Simulation of a Two-Layer Boundary-Layer Cloud System from the Arctic Ocean 2018 Expedition". In: *Atmospheric Chem. Phys.* 23.12, pp. 7033–7055. ISSN: 1680-7316. DOI: 10.5194/acp-23-7033-2023.

climate.gov (2020). *2020 Arctic Sea Ice Minimum Second Lowest on Record*. https://www.climate.gov/news-features/featured-images/2020-arctic-sea-ice-minimum-second-lowest-record. Accessed 2026-02-23.

Cotton, W., G. Bryan and S. van den Heever (2010). *Storm and Cloud Dynamics*. Academic Press.

Creamean, J. M., K. Barry, T. C. J. Hill, C. Hume, P. J. DeMott, M. D. Shupe, S. Dahlke, S. Willmes, J. Schmale, I. Beck, C. J. M. Hoppe, A. Fong, E. Chamberlain, J. Bowman, R. Scharien and O. Persson (2022). "Annual Cycle Observations of Aerosols Capable of Ice Formation in Central Arctic Clouds". In: *Nat Commun* 13.1, p. 3537. ISSN: 2041-1723. DOI: 10.1038/s41467-022-31182-x.

Curry, J. A. (1986). "Interactions among Turbulence, Radiation and Microphysics in Arctic Stratus Clouds". In: *J. Atmospheric Sci.* 43.1, pp. 90–106. ISSN: 0022-4928, 1520-0469. DOI: 10.1175/1520-0469(1986)043<0090:IATRAM>2.0.CO;2.

Curry, J. A. and E. E. Ebert (1992). "Annual Cycle of Radiation Fluxes over the Arctic Ocean: Sensitivity to Cloud Optical Properties". In: *J. Clim.* 5.11, pp. 1267–1280. ISSN: 0894-8755, 1520-0442. DOI: 10.1175/1520-0442(1992)005<1267:ACORFO>2.0.CO;2.

de Boer, G., H. Morrison, M. D. Shupe and R. Hildner (2011). "Evidence of Liquid Dependent Ice Nucleation in High-Latitude Stratiform Clouds from Surface Remote Sensors". In: *Geophys. Res. Lett.* 38.1. ISSN: 1944-8007. DOI: 10.1029/2010GL046016.

DeMott, P. J., A. J. Prenni, X. Liu, S. M. Kreidenweis, M. D. Petters, C. H. Twohy, M. S. Richardson, T. Eidhammer and D. C. Rogers (2010). "Predicting Global Atmospheric Ice Nuclei Distributions and Their Impacts on Climate". In: *Proceedings of the National Academy of Sciences*

107.25, pp. 11217–11222. ISSN: 0027-8424, 1091-6490. DOI: 10.1073/pnas.0910818107.

Dipankar, A., B. Stevens, R. Heinze, C. Moseley, G. Zängl, M. Giorgetta and S. Brdar (2015). "Large eddy simulation using the general circulation model ICON". In: *Journal of Advances in Modeling Earth Systems* 7, pp. 963–986. DOI: 10.1002/2015MS000431.

Eastman, R. and S. G. Warren (2010). "Interannual Variations of Arctic Cloud Types in Relation to Sea Ice". In: *J. Clim.* 23.15, pp. 4216–4232. ISSN: 0894-8755, 1520-0442. DOI: 10.1175/2010JCLI3492.1.

Eriksson, P., R. Ekelund, J. Mendrok, M. Brath, O. Lemke and S. A. Buehler (2018). "A general database of hydrometeor single scattering properties at microwave and sub-millimetre wavelengths". In: *Earth System Science Data* 10.3, pp. 1301–1326. DOI: 10.5194/essd-10-1301-2018.

Findeisen, W. (1938). "Kolloid-meteorologische Vorgänge bei Niederschlagsbildung". In: *Meteor. Z.* 55, pp. 121–133.

Fu, Q. and K. N. Liou (1993). "Parameterization of the Radiative Properties of Cirrus Clouds". In: *J. Atmospheric Sci.* 50.13, pp. 2008–2025.

Fu, Q., K. N. Liou, M. C. Cribb, T. P. Charlock and A. Grossman (1997). "Multiple Scattering Parameterization in Thermal Infrared Radiative Transfer". In: *J. Atmospheric Sci.* 54.24, pp. 2799–2812. ISSN: 0022-4928, 1520-0469. DOI: 10.1175/1520-0469(1997)054<2799:MSPITI>2.0.CO;2.

Garimella, S., T. B. Kristensen, K. Ignatius, A. Welti, J. Voigtländer, G. R. Kulkarni, F. Sagan, G. L. Kok, J. Dorsey, L. Nichman, D. A. Rothenberg, M. Rösch, A. C. R. Kirchgäßner, R. Ladkin, H. Wex, T. W. Wilson, L. A. Ladino, J. P. D. Abbatt, O. Stetzer, U. Lohmann, F. Stratmann and D. J. Cziczo (2016). "The SPectrometer for Ice Nuclei (SPIN): An Instrument to Investigate Icenucleation". In: *Atmos. Meas. Tech.* 9.7, pp. 2781–2795. ISSN: 1867-8548. DOI: 10.5194/amt-9-2781-2016.

Gómez Martín, J. C., D. Guirado, E. Frattin, M. Bermudez-Edo, P. Cariñanos Gonzalez, F. J. Olmo Reyes, T. Nousiainen, P. J. Gutiérrez, F. Moreno and O. Muñoz (2021). "On the Application of Scattering Matrix Measurements to Detection and Identification of Major Types of Airborne Aerosol Particles: Volcanic Ash, Desert Dust and Pollen". In: *Journal of Quantitative Spectroscopy and Radiative Transfer* 271, p. 107761. ISSN: 0022-4073. DOI: 10.1016/j.jqsrt.2021.107761.

Goosse, H., P. Y. Barriat, W. Lefebvre, M. F. Loutre and V. Zunz (2008). *Introduction to Climate Dynamics and Climate Modeling*. Cambridge University Press.

Goosse, H., J. E. Kay, K. C. Armour, A. Bodas-Salcedo, H. Chepfer, D. Docquier, A. Jonko, P. J. Kushner, O. Lecomte, F. Massonnet, H.-S. Park, F. Pithan, G. Svensson and M. Vancoppenolle (2018). "Quantifying Climate Feedbacks in Polar Regions". In: *Nat Commun* 9.1, p. 1919. ISSN: 2041-1723. DOI: 10.1038/s41467-018-04173-0.

Gu, Y., J. Farrara, K. N. Liou and C. R. Mechoso (2003). "Parameterization of Cloud–Radiation Processes in the UCLA General Circulation Model". In: *J. Clim.* 16.20, pp. 3357–3370. ISSN: 0894-8755, 1520-0442. DOI: 10.1175/1520-0442(2003)016<3357:POCPIT>2.0.CO;2.

Hallett, J. and S. C. Mossop (1974). "Production of Secondary Ice Particles during the Riming Process". In: *Nature* 249.5452, pp. 26–28. ISSN: 0028-0836. DOI: 10.1038/249026a0.

Hartmann, D. L. (1994). *Global Physical Climatology*. Academic Press.

Hess, M. and M. Wiegner (1994). "COP: a data library of optical properties of hexagonal ice crystals". In: *Appl. Opt.* 33.33, pp. 7740–7746. DOI: 10.1364/AO.33.007740.

Heus, T., C. C. van Heerwaarden, H. J. Jonker, A. P. Siebesma, S. Axelsen, K. V. D. Dries, O. Geoffroy, A. F. Moene, D. Pino, S. R. D. Roode and J. V.-G. de Arellano (2010). "Formulation of the Dutch Atmospheric Large-Eddy Simulation (DALES) and overview of its applications". In: *Geosci. Model Dev.* 3, pp. 415–444.

Hobbs, P. V. and A. L. Rangno (1985). "Ice Particle Concentrations in Clouds". In: *J. Atmospheric Sci.* 42.23, pp. 2523–2549. ISSN: 0022-4928, 1520-0469. DOI: 10.1175/1520-0469(1985)042<2523:IPCIC>2.0.CO;2.

Hoose, C. and O. Möhler (2012). "Heterogeneous Ice Nucleation on Atmospheric Aerosols: A Review of Results from Laboratory Experiments". In: *Atmos. Chem. Phys.* 12.20, pp. 9817–9854. ISSN: 1680-7324. DOI: 10.5194/acp-12-9817-2012.

Hoose, C., J. E. Kristjánsson, J.-P. Chen and A. Hazra (2010). "A Classical-Theory-Based Parameterization of Heterogeneous Ice Nucleation by Mineral Dust, Soot, and Biological Particles in a Global Climate Model". In: *J. Atmospheric Sci.* 67.8, pp. 2483–2503. ISSN: 0022-4928, 1520-0469. DOI: 10.1175/2010JAS3425.1.

Ickes, L., A. Welti and U. Lohmann (2017). "Classical Nucleation Theory of Immersion Freezing: Sensitivity of Contact Angle Schemes to Thermodynamic and Kinetic Parameters". In: *Atmospheric Chem. Phys.* 17.3, pp. 1713–1739. ISSN: 16807324. DOI: 10.5194/acp-17-1713-2017.

Igel, A. L., A. M. L. Ekman, C. Leck, M. Tjernström, J. Savre and J. Sedlar (2017). "The Free Troposphere as a Potential Source of Arctic Boundary Layer Aerosol Particles". In: *Geophys. Res. Lett.* 44.13, pp. 7053–7060. ISSN: 0094-8276. DOI: 10.1002/2017GL073808.

IPCC (2021). *Climate Change 2021: The Physical Science Basis. Contribution of Working Group I to the Sixth Assessment Report of the Intergovernmental Panel on Climate Change*. Ed. by V. Masson-Delmotte, P. Zhai, A. Pirani, S. L. Connors, C. Péan, S. Berger, N. Caud, Y. Chen, L. Goldfarb, M. I. Gomis, M. Huang, K. Leitzell, E. Lonnoy, J. B. R. Matthews, T. K. Maycock, T. Waterfield, O. Yelekçi, R. Yu and B. Zhou. Cambridge University Press.

Isaac, G. A. and R. H. Douglas (1971). *Frequency Distributions of Ice Nucleus Concentrations*.

Jimenez, C., A. Ansmann, K. Ohneiser, H. Griesche, R. Engelmann, M. Radenz, J. Hofer, D. Althausen, D. A. Knopf, S. Dahlke, J. Bühl, H. Baars, P. Seifert and U. Wandinger (2025). "MOSAiC Studies of Long-Lasting Mixed-Phase Cloud Events and Analysis of the Liquid-Phase Properties of Arctic Clouds". In: *Atmospheric Chem. Phys.* 25.20, pp. 12955–12981. ISSN: 1680-7316. DOI: 10.5194/acp-25-12955-2025.

Jozef, G. C., J. J. Cassano, S. Dahlke, M. Dice, C. J. Cox and G. de Boer (2024). "An Overview of the Vertical Structure of the Atmospheric Boundary Layer in the Central Arctic during MOSAiC". In: *Atmospheric Chem. Phys.* 24.2, pp. 1429–1450. ISSN: 1680-7316. DOI: 10.5194/acp-24-1429-2024.

Juliano, T. W., F. Tornow, A. M. Fridlind, A. S. Ackerman, G. S. Elsaesser, B. Geerts, C. P. Lackner, D. Painemal, I. Silber, M. Ovchinnikov, G. Svensson, M. Tjernström, P. Wu, A. Baró Pérez, P. Bogenschutz, D. Chechin, K. K. Chandrakar, J. Chylik, A. Debolskiy, R. Fadeev, A. Gupta, L. Ickes, M. Karalis, M. Köhler, B. Kosović, P. Kuma, W. Li, E. Mortikov, H. Morrison, R. A. J. Neggers, A. Possner, T. Raatikainen, S. Romakkaniemi, N. Schnierstein, S.-i. Shima, N. Silin, M. Tolstykh, L. Xue, M. Zhang and X. Zheng (2026). "The Cold-Air Outbreaks in the Marine Boundary Layer Experiment Model-Observation Intercomparison Project (COMBLE-MIP), Part I: Model Specification, Observational Constraints, and Preliminary Findings". In: *EGUsphere*, pp. 1–52. DOI: 10.5194/egusphere-2025-6217.

Kadantsev, E., E. Mortikov and S. Zilitinkevich (2021). "The resistance law for stably stratified atmospheric planetary boundary layers". In: *Quarterly Journal of the Royal Meteorological Society* 147, pp. 2233–2243.

Kanji, Z. A., L. A. Ladino, H. Wex, Y. Boose, M. Burkert-Kohn, D. J. Cziczo and M. Krämer (2017). "Overview of Ice Nucleating Particles". In: *Meteorol. Monogr.* 58.1, pp. 1.1–1.33. DOI: 10.1175/AMSMONOGRAPHS-D-16-0006.1.

Khairoutdinov, M. F. and D. A. Randall (2003). "Cloud resolving modeling of the ARM summer 1997 IOP: Model formulation, results, uncertainties, and sensitivities". In: *Journal of the Atmospheric Sciences* 60, pp. 607–625.

Korolev, A. and T. Leisner (2020). "Review of Experimental Studies of Secondary Ice Production". In: *Atmos. Chem. Phys.* 20.20, pp. 11767–11797. ISSN: 1680-7324. DOI: 10.5194/acp-20-11767-2020.

Kristi Wallace, U.S. Geological Survey (2015). *Scanning Electron Microscope image of volcanic ash*. https://www.usgs.gov/media/images/scanning-electron-microscope-image-volcanic-ash. Accessed 2026-05-02.

Köhler, H. (1936). "The nucleus in and the growth of hygroscopic droplets". In: *Transactions of the Faraday Society* 32, pp. 1152–1161.

Lauber, A., A. Kiselev, T. Pander, P. Handmann and T. Leisner (2018). "Secondary Ice Formation during Freezing of Levitated Droplets". In: *J. Atmospheric Sci.* 75.8, pp. 2815–2826. ISSN: 0022-4928. DOI: 10.1175/JAS-D-18-0052.1.

Libbrecht, K. G. (2019). *Snow Crystals*.

Loewe, K., A. M. L. Ekman, M. Paukert, J. Sedlar, M. Tjernström and C. Hoose (2017). "Modelling Micro- and Macrophysical Contributors to the Dissipation of an Arctic Mixed-Phase Cloud during the Arctic Summer Cloud Ocean Study (ASCOS)". In: *Atmospheric Chem. Phys.* 17.11, pp. 6693–6704. ISSN: 1680-7324. DOI: 10.5194/acp-17-6693-2017.

Lohmann, U., F. Lüönd and F. Mahrt (2016). *An Introduction to Clouds: From the Microscale to Climate*. Cambridge University Press.

Matus, A. V. and T. S. L'Ecuyer (2017). "The Role of Cloud Phase in Earth's Radiation Budget". In: *J. Geophys. Res. Atmospheres* 122.5, pp. 2559–2578. ISSN: 2169-8996. DOI: 10.1002/2016JD025951.

Mauritsen, T., J. Sedlar, M. Tjernström, C. Leck, M. Martin, M. Shupe, S. Sjogren, B. Sierau, P. O. G. Persson, I. M. Brooks and E. Swietlicki (2011). "An Arctic CCN-limited Cloud-Aerosol Regime". In: *Atmospheric Chem. Phys.* 11.1, pp. 165–173. ISSN: 1680-7316. DOI: 10.5194/acp-11-165-2011.

McFarquhar, G. M., C. S. Bretherton, R. Marchand, A. Protat, P. J. DeMott, S. P. Alexander, G. C. Roberts, C. H. Twohy, D. Toohey, S. Siems, Y. Huang, R. Wood, R. M. Rauber, S. Lasher-Trapp, J. Jensen, J. L. Stith, J. Mace, J. Um, E. Järvinen, M. Schnaiter, A. Gettelman, K. J. Sanchez, C. S. McCluskey, L. M. Russell, I. L. McCoy, R. L. Atlas, C. G. Bardeen, K. A. Moore, T. C. J. Hill, R. S. Humphries, M. D. Keywood, Z. Ristovski, L. Cravigan, R. Schofield, C. Fairall, M. D. Mallet, S. M. Kreidenweis, B. Rainwater, J. D'Alessandro, Y. Wang, W. Wu, G. Saliba, E. J. T. Levin, S. Ding, F. Lang, S. C. H. Truong, C. Wolff, J. Haggerty, M. J. Harvey, A. R. Klekociuk and A. McDonald (2021). "Observations of Clouds, Aerosols, Precipitation, and Surface Radiation over the Southern Ocean: An Overview of CAPRICORN, MARCUS, MICRE, and SOCRATES". In: *Bulletin of the American Meteorological Society*. DOI: 10.1175/BAMS-D-20-0132.1.

Morrison, H., G. De Boer, G. Feingold, J. Harrington, M. D. Shupe and K. Sulia (2012). "Resilience of Persistent Arctic Mixed-Phase Clouds". In: *Nature Geosci* 5.1, pp. 11–17. ISSN: 1752-0894, 1752-0908. DOI: 10.1038/ngeo1332.

Morrison, H. and J. A. Milbrandt (2015). "Parameterization of Cloud Microphysics Based on the Prediction of Bulk Ice Particle Properties. Part I: Scheme Description and Idealized Tests". In: *J. Atmospheric Sci.* 72.1, pp. 287–311. ISSN: 0022-4928. DOI: 10.1175/JAS-D-14-0065.1.

Mortikov, E. V., A. V. Glazunov and V. N. Lykosov (2019). "Numerical study of plane Couette flow: turbulence statistics and the structure of pressure-strain correlations". In: *Russian Journal of Numerical Analysis and Mathematical Modelling* 34, pp. 119–132. DOI: 10.1515/rnam-2019-0010.

Mülmenstädt, J., O. Sourdeval, J. Delanoë and J. Quaas (2015). "Frequency of Occurrence of Rain from Liquid-, Mixed-, and Ice-Phase Clouds Derived from A-Train Satellite Retrievals". In: *Geophys. Res. Lett.* 42.15, pp. 6502–6509. ISSN: 1944-8007. DOI: 10.1002/2015GL064604.

Nakaya, U. (1954). *Snow crystals: natural and artificial*. Harvard University Press.

NASA (2009). *Sea Salt Aerosols*. https://svs.gsfc.nasa.gov/10390/. Accessed 2026-05-02.

NASA/Goddard Space Flight Center (2009). *Scanning Electron Microscope Still Image of Pollen Particles*. https://svs.gsfc.nasa.gov/10394. Accessed 2026-05-02.

National Snow and Ice Data Center (2026). *Sea ice index: extent and concentration trends*. https://nsidc.org/data/bist. Accessed 2026-04-10.

Niemand, M., O. Möhler, B. Vogel, H. Vogel, C. Hoose, P. Connolly, H. Klein, H. Bingemer, P. Demott, J. Skrotzki and T. Leisner (2012). "A Particle-Surface-Area-Based Parameterization of Immersion Freezing on Desert Dust Particles". In: *J. Atmospheric Sci.* 69.10, pp. 3077–3092. ISSN: 00224928. DOI: 10.1175/JAS-D-11-0249.1.

Nishizawa, S., H. Yashiro, Y. Sato, Y. Miyamoto and H. Tomita (2015). "Influence of Grid Aspect Ratio on Planetary Boundary Layer Turbulence in Large-Eddy Simulations". In: *Geosci. Model Dev.* 8.10, pp. 3393–3419. DOI: 10.5194/gmd-8-3393-2015.

Ott, W. R. (1990). "A Physical Explanation of the Lognormality of Pollutant Concentrations". In: *J. Air Waste Manag. Assoc.* 40.10, pp. 1378–1383. ISSN: 10473289. DOI: 10.1080/10473289.1990.10466789.

Pasquier, J. T., J. Henneberger, F. Ramelli, A. Lauber, R. O. David, J. Wieder, T. Carlsen, R. Gierens, M. Maturilli and U. Lohmann (2022). "Conditions Favorable for Secondary Ice Production in Arctic Mixed-Phase Clouds". In: *Atmospheric Chem. Phys.* 22.23, pp. 15579–15601. ISSN: 1680-7316. DOI: 10.5194/acp-22-15579-2022.

Penner, J. E., D. H. Lister, D. J. Griggs, D. J. Dokken and M. McFarland, eds. (1999). *Aviation and the Global Atmosphere. A Special Report of Working Group III of the Intergovernmental Panel on Climate Change*. Cambridge University Press.

Philipp, D., M. Stengel and B. Ahrens (2020). "Analyzing the Arctic Feedback Mechanism between Sea Ice and Low-Level Clouds Using 34 Years of Satellite Observations". In: *J. Clim.* 33.17, pp. 7479–7501. ISSN: 0894-8755, 1520-0442. DOI: 10.1175/JCLI-D-19-0895.1.

Phillips, V. T. J., P. J. DeMott and C. Andronache (2008). "An Empirical Parameterization of Heterogeneous Ice Nucleation for Multiple Chemical Species of Aerosol". In: *J. Atmospheric Sci.* 65.9, pp. 2757–2783. ISSN: 1520-0469, 0022-4928. DOI: 10.1175/2007JAS2546.1.

Phillips, V. T. J., S. Patade, J. Gutierrez and A. Bansemer (2018). "Secondary Ice Production by Fragmentation of Freezing Drops: Formulation and Theory". In: *J. Atmospheric Sci.* 75.9, pp. 3031–3070. ISSN: 0022-4928. DOI: 10.1175/JAS-D-17-0190.1.

Phillips, V. T. J., J.-I. Yano, M. Formenton, E. Ilotoviz, V. Kanawade, I. Kudzotsa, J. Sun, A. Bansemer, A. G. Detwiler, A. Khain and S. A. Tessendorf (2017a). "Ice Multiplication by Breakup in Ice–Ice Collisions. Part II: Numerical Simulations". In: *J. Atmospheric Sci.* 74.9, pp. 2789–2811. ISSN: 0022-4928. DOI: 10.1175/JAS-D-16-0223.1.

Phillips, V. T. J., J.-I. Yano and A. Khain (2017b). "Ice Multiplication by Breakup in Ice–Ice Collisions. Part I: Theoretical Formulation". In: *J. Atmospheric Sci.* 74.6, pp. 1705–1719. ISSN: 0022-4928. DOI: 10.1175/JAS-D-16-0224.1.

Pohorsky, R., H. Guy, I. M. Brooks, L. Haberstock, N. Fauré, P. Zieger, J. Kojoj, S. Murto, R. Calmer, B. Heutte, M. Lonardi, E. S. Thomson, M. Tjernström, J. Creamean, A. Nenes and J. Schmale (2026). "Contribution of Free Tropospheric Aerosols to Arctic Low-Level Cloud Droplets Formation and Longwave Radiative Forcing". In: *EGUsphere*, pp. 1–37. DOI: 10.5194/egusphere-2026-1068.

Pruppacher, H. R. and J. D. Klett (2010). *Microphysics of Clouds and Precipitation*. 2. Kluwer Academic.

Rantanen, M., A. Y. Karpechko, A. Lipponen, K. Nordling, O. Hyvärinen, K. Ruosteenoja, T. Vihma and A. Laaksonen (2022). "The Arctic Has Warmed

Nearly Four Times Faster than the Globe since 1979". In: *Commun Earth Environ* 3.1, p. 168. ISSN: 2662-4435. DOI: 10.1038/s43247-022-00498-3.

Raoult, F.-M. (1886). "Loi générale des tensions de vapeur des dissolvants". In: *Comptes rendus* 104, pp. 1430–1433.

Reisner, J., R. M. Rasmussen and R. T. Bruintjes (1998). "Explicit Forecasting of Supercooled Liquid Water in Winter Storms Using the MM5 Mesoscale Model". In: *Q. J. R. Meteorol. Soc.* 124.548, pp. 1071–1107. ISSN: 00359009. DOI: 10.1256/smsqj.54803.

Rogers, D. C. (1988). "Development of a Continuous Flow Thermal Gradient Diffusion Chamber for Ice Nucleation Studies". In: *Atmospheric Research* 22.2, pp. 149–181. ISSN: 0169-8095. DOI: 10.1016/0169-8095(88)90005-1.

Savre, J. and A. M. L. Ekman (2015). "Large-Eddy Simulation of Three Mixed-Phase Cloud Events during ISDAC: Conditions for Persistent Heterogeneous Ice Formation". In: *J. Geophys. Res. Atmospheres* 120.15, pp. 7699–7725. ISSN: 2169-8996. DOI: 10.1002/2014JD023006.

Savre, J., A. M. L. Ekman and G. Svensson (2014). "Technical Note: Introduction to MIMICA, a Large-Eddy Simulation Solver for Cloudy Planetary Boundary Layers". In: *J. Adv. Model. Earth Syst.* 6.3, pp. 630–649. ISSN: 19422466. DOI: 10.1002/2013MS000292.

Schäfer, B., R. O. David, P. Georgakaki, J. T. Pasquier, G. Sotiropoulou and T. Storelvmo (2024). "Simulations of Primary and Secondary Ice Production during an Arctic Mixed-Phase Cloud Case from the Ny-Ålesund Aerosol Cloud Experiment (NASCENT) Campaign". In: *Atmospheric Chem. Phys.* 24.12, pp. 7179–7202. ISSN: 1680-7316. DOI: 10.5194/acp-24-7179-2024.

Screen, J. A. and I. Simmonds (2010). "The Central Role of Diminishing Sea Ice in Recent Arctic Temperature Amplification". In: *Nature* 464.7293, pp. 1334–1337. ISSN: 1476-4687. DOI: 10.1038/nature09051.

Sedlar, J., M. Tjernström, T. Mauritsen, M. D. Shupe, I. M. Brooks, P. O. G. Persson, C. E. Birch, C. Leck, A. Sirevaag and M. Nicolaus (2011). "A Transitioning Arctic Surface Energy Budget: The Impacts of Solar Zenith Angle, Surface Albedo and Cloud Radiative Forcing". In: *Clim Dyn* 37.7, pp. 1643–1660. ISSN: 1432-0894. DOI: 10.1007/s00382-010-0937-5.

Seifert, A. and K. D. Beheng (2006). "A Two-Moment Cloud Microphysics Parameterization for Mixed-Phase Clouds. Part 1: Model Description". In: *Meteorol. Atmospheric Phys.* 92.1-2, pp. 45–66. ISSN: 01777971. DOI: 10.1007/s00703-005-0112-4.

Seinfeld, J. and S. Pandis (2016). *Atmospheric Chemistry and Physics: From Air Pollution to Climate Change*. Third. John Wiley & Sons, Inc.

Serreze, M. C. and R. G. Barry (2011). "Processes and Impacts of Arctic Amplification: A Research Synthesis". In: *Global and Planetary Change* 77.1, pp. 85–96. ISSN: 0921-8181. DOI: 10.1016/j.gloplacha.2011.03.004.

Shupe, M. D., P. O. Persson, I. M. Brooks, M. Tjernström, J. Sedlar, T. Mauritsen, S. Sjogren and C. Leck (2013). "Cloud and Boundary Layer Interactions over the Arctic Sea Ice in Late Summer". In: *Atmospheric Chem. Phys.* DOI: 10.5194/acp-13-9379-2013.

Shupe, M. D. (2011). "Clouds at Arctic Atmospheric Observatories. Part II: Thermodynamic Phase Characteristics". In: *J. Appl. Meteorol. Climatol.*

50.3, pp. 645–661. ISSN: 1558-8424, 1558-8432. DOI: 10.1175/2010JAMC2468.1.

Shupe, M. D. and J. M. Intrieri (2004). "Cloud Radiative Forcing of the Arctic Surface: The Influence of Cloud Properties, Surface Albedo, and Solar Zenith Angle". In: *J. Climate* 17.3, pp. 616–628. ISSN: 0894-8755, 1520-0442. DOI: 10.1175/1520-0442(2004)017<0616:CRFOTA>2.0.CO;2.

Shupe, M. D., P. Kollias, P. O. G. Persson and G. M. McFarquhar (2008). "Vertical Motions in Arctic Mixed-Phase Stratiform Clouds in: Journal of the Atmospheric Sciences Volume 65 Issue 4 (2008)". In: *J. Atmos. Sci.* 65.4, pp. 1304–1322. DOI: 10.1175/2007JAS2479.1.

Shupe, M. D., S. Y. Matrosov and T. Uttal (2006). "Arctic Mixed-Phase Cloud Properties Derived from Surface-Based Sensors at SHEBA". In: *J. Atmospheric Sci.* 63.2, pp. 697–711. ISSN: 0022-4928, 1520-0469. DOI: 10.1175/JAS3659.1.

Shupe, M. D., V. P. Walden, E. Eloranta, T. Uttal, J. R. Campbell, S. M. Starkweather and M. Shiobara (2011). "Clouds at Arctic Atmospheric Observatories. Part I: Occurrence and Macrophysical Properties". In: *J. Appl. Meteorol. Climatol.* 50.3, pp. 626–644. ISSN: 1558-8424, 1558-8432. DOI: 10.1175/2010JAMC2467.1.

Shupe, M. D. et al. (2022). "Overview of the MOSAiC Expedition: Atmosphere". In: *Elementa: Science of the Anthropocene* 10.1, p. 00060. ISSN: 2325-1026. DOI: 10.1525/elementa.2021.00060.

Skamarock, W. C., J. B. Klemp, J. Dudhia, D. O. Gill, Z. Liu, J. Berner, W. Wang, J. G. Powers, M. G. Duda, D. M. Barker and X.-Y. Huang (2019). *A Description of the Advanced Research WRF Model Version 4*. NCAR Technical Note NCAR/TN-556+STR. National Center for Atmospheric Research.

Solomon, A., M. D. Shupe, P. O. G. Persson and H. Morrison (2011). "Moisture and Dynamical Interactions Maintaining Decoupled Arctic Mixed-Phase Stratocumulus in the Presence of a Humidity Inversion". In: *Atmospheric Chem. Phys.* 11.19, pp. 10127–10148. ISSN: 1680-7316. DOI: 10.5194/acp-11-10127-2011.

Solomon, S. (1988). "The Mystery of the Antarctic Ozone "Hole"". In: *Rev. Geophys.* 26.1, pp. 131–148. ISSN: 1944-9208. DOI: 10.1029/RG026i001p00131.

Sotiropoulou, G., J. Sedlar, M. Tjernström, M. D. Shupe, I. M. Brooks and P. O. G. Persson (2014). "The Thermodynamic Structure of Summer Arctic Stratocumulus and the Dynamic Coupling to the Surface". In: *Atmospheric Chem. Phys.* 14.22, pp. 12573–12592. ISSN: 1680-7324. DOI: 10.5194/acp-14-12573-2014.

Sotiropoulou, G., S. Sullivan, J. Savre, G. Lloyd, T. Lachlan-Cope, A. M. L. Ekman and A. Nenes (2020). "The Impact of Secondary Ice Production on Arctic Stratocumulus". In: *Atmospheric Chem. Phys.* 20.3, pp. 1301–1316. ISSN: 1680-7324. DOI: 10.5194/acp-20-1301-2020.

Spracklen, D. V., K. S. Carslaw, J. Merikanto, G. W. Mann, C. L. Reddington, S. Pickering, J. A. Ogren, E. Andrews, U. Baltensperger, E. Weingartner, M. Boy, M. Kulmala, L. Laakso, H. Lihavainen, N. Kivekäs, M. Komppula, N. Mihalopoulos, G. Kouvarakis, S. G. Jennings, C. O'Dowd, W. Birmili,

A. Wiedensohler, R. Weller, J. Gras, P. Laj, K. Sellegri, B. Bonn, R. Krejci, A. Laaksonen, A. Hamed, A. Minikin, R. M. Harrison, R. Talbot and J. Sun (2010). "Explaining Global Surface Aerosol Number Concentrations in Terms of Primary Emissions and Particle Formation". In: *Atmospheric Chem. Phys.* 10.10, pp. 4775–4793. ISSN: 1680-7316. DOI: 10.5194/acp-10-4775-2010.

Sterzinger, L. J., J. Sedlar, H. Guy, R. R. Neely III and A. L. Igel (2022). "Do Arctic Mixed-Phase Clouds Sometimes Dissipate Due to Insufficient Aerosol? Evidence from Comparisons between Observations and Idealized Simulations". In: *Atmospheric Chem. Phys.* 22.13, pp. 8973–8988. ISSN: 1680-7316. DOI: 10.5194/acp-22-8973-2022.

Stevens, B. (2002). "Entrainment in stratocumulus-topped mixed layers". In: *Quarterly Journal of the Royal Meteorological Society: A journal of the atmospheric sciences, applied meteorology and physical oceanography* 128, pp. 2663–2690.

Stevens, B., C.-H. Moeng, A. S. Ackerman, C. S. Bretherton, A. Chlond, S. de Roode, J. Edwards, J.-C. Golaz, H. Jiang, M. Khairoutdinov et al. (2005). "Evaluation of large-eddy simulations via observations of nocturnal marine stratocumulus". In: *Monthly Weather Review* 133, pp. 1443–1462.

Stevens, B., C.-H. Moeng and P. P. Sullivan (1999). "Large-eddy simulations of radiatively driven convection: Sensitivities to the representation of small scales". In: *Journal of the Atmospheric Sciences* 56, pp. 3963–3984.

Stevens, B. and A. Seifert (2008). "Understanding macrophysical outcomes of microphysical choices in simulations of shallow cumulus convection". In: *Journal of the Meteorological Society of Japan. Ser. II* 86A, pp. 143–162. DOI: 10.2151/jmsj.86A.143.

Stevens, R. G., K. Loewe, C. Dearden, A. Dimitrelos, A. Possner, G. K. Eirund, T. Raatikainen, A. A. Hill, B. J. Shipway, J. Wilkinson, S. Romakkaniemi, J. Tonttila, A. Laaksonen, H. Korhonen, P. Connolly, U. Lohmann, C. Hoose, A. M. L. Ekman, K. S. Carslaw and P. R. Field (2018). "A Model Intercomparison of CCN-limited Tenuous Clouds in the High Arctic". In: *Atmospheric Chem. Phys.* 18.15, pp. 11041–11071. ISSN: 1680-7324. DOI: 10.5194/acp-18-11041-2018.

Sullivan, S. C., C. Barthlott, J. Crosier, I. Zhukov, A. Nenes and C. Hoose (2018). "The Effect of Secondary Ice Production Parameterization on the Simulation of a Cold Frontal Rainband". In: *Atmospheric Chem. Phys.* 18.22, pp. 16461–16480. ISSN: 1680-7324. DOI: 10.5194/acp-18-16461-2018.

Thomson, W. (1871). "On the equilibrium of vapour at a curved surface of liquid". In: *Philosophical Magazine* 42.282, pp. 448–452.

Tjernström, M., C. E. Birch, I. M. Brooks, M. D. Shupe, P. O. G. Persson, J. Sedlar, T. Mauritsen, C. Leck, J. Paatero, M. Szczodrak and C. R. Wheeler (2012). "Meteorological Conditions in the Central Arctic Summer during the Arctic Summer Cloud Ocean Study (ASCOS)". In: *Atmospheric Chem. Phys.* 12.15, pp. 6863–6889. ISSN: 1680-7324. DOI: 10.5194/acp-12-6863-2012.

Tjernström, M., C. Leck, C. E. Birch, J. W. Bottenheim, B. J. Brooks, I. M. Brooks, L. Bäcklin, R. Y.-W. Chang, G. de Leeuw, L. Di Liberto, S. de la Rosa, E. Granath, M. Graus, A. Hansel, J. Heintzenberg, A. Held, A.

Hind, P. Johnston, J. Knulst, M. Martin, P. A. Matrai, T. Mauritsen, M. Müller, S. J. Norris, M. V. Orellana, D. A. Orsini, J. Paatero, P. O. G. Persson, Q. Gao, C. Rauschenberg, Z. Ristovski, J. Sedlar, M. D. Shupe, B. Sierau, A. Sirevaag, S. Sjogren, O. Stetzer, E. Swietlicki, M. Szczodrak, P. Vaattovaara, N. Wahlberg, M. Westberg and C. R. Wheeler (2014). "The Arctic Summer Cloud Ocean Study (ASCOS): Overview and Experimental Design". In: *Atmospheric Chem. Phys.* 14.6, pp. 2823–2869. ISSN: 1680-7324. DOI: 10.5194/acp-14-2823-2014.

Tjernström, M. and P. Zieger, eds. (2025). *Expedition report Atmospheric rivers and the onset of Arctic melt, ARTofMELT, 2023 with icebreaker Oden*. Swedish Polar Research Secretariat. ISBN: 978-91-519-5134-8.

Uttal, T., J. A. Curry, M. G. McPhee, D. K. Perovich, R. E. Moritz, J. A. Maslanik, P. S. Guest, H. L. Stern, J. A. Moore, R. Turenne, A. Heiberg, M. C. Serreze, D. P. Wylie, O. G. Persson, C. A. Paulson, C. Halle, J. H. Morison, P. A. Wheeler, A. Makshtas, H. Welch, M. D. Shupe, J. M. Intrieri, K. Stamnes, R. W. Lindsey, R. Pinkel, W. S. Pegau, T. P. Stanton and T. C. Grenfeld (2002). "Surface Heat Budget of the Arctic Ocean". In: *Bull. Am. Meteorol. Soc.* 83.2, pp. 255–276. ISSN: 0003-0007, 1520-0477. DOI: 10.1175/1520-0477(2002)083<0255:SHBOTA>2.3.CO;2.

Vali, G. (2014). "Interpretation of Freezing Nucleation Experiments: Singular and Stochastic; Sites and Surfaces". In: *Atmos. Chem. Phys.* 14.11, pp. 5271–5294. ISSN: 1680-7324. DOI: 10.5194/acp-14-5271-2014.

Vardiman, L. (1978). "The Generation of Secondary Ice Particles in Clouds by Crystal–Crystal Collision". In: *J. Atmospheric Sci.* 35.11, pp. 2168–2180. ISSN: 0022-4928, 1520-0469. DOI: 10.1175/1520-0469(1978)035<2168:TGOSIP>2.0.CO;2.

Voevodin, V. V., A. V. Debolskiy and E. V. Mortikov (2023). "Facilitating the Process of Performance Analysis of HPC Applications". In: *Lobachevskii Journal of Mathematics* 44, pp. 3177–3189. DOI: 10.1134/S1995080223080589.

Vüllers, J., P. Achtert, I. M. Brooks, M. Tjernström, J. Prytherch, A. Burzik and R. Neely III (2021). "Meteorological and Cloud Conditions during the Arctic Ocean 2018 Expedition". In: *Atmospheric Chem. Phys.* 21.1, pp. 289–314. ISSN: 1680-7316. DOI: 10.5194/acp-21-289-2021.

Wang, C. and J. S. Chang (1993). "A Three-Dimensional Numerical Model of Cloud Dynamics, Microphysics, and Chemistry: 1. Concepts and Formulation". In: *J. Geophys. Res.* 98.D8, p. 14827. ISSN: 0148-0227. DOI: 10.1029/92JD01393.

Wang, X. and J. R. Key (2005). "Arctic Surface, Cloud, and Radiation Properties Based on the AVHRR Polar Pathfinder Dataset. Part II: Recent Trends". In: *J. Clim.* 18.14, pp. 2575–2593. ISSN: 0894-8755, 1520-0442. DOI: 10.1175/JCLI3439.1.

Wegener, A. (1911). *Thermodynamik der Atmosphäre*. Leipzig, Germany: J. A. Barth.

Welti, A., K. Müller, Z. L. Fleming and F. Stratmann (2018). "Concentration and Variability of Ice Nuclei in the Subtropical Maritime Boundary Layer".

In: *Atmospheric Chem. Phys.* 18.8. ISSN: 16807324. DOI: 10.5194/acp-18-5307-2018.

Westbrook, C. D. and A. J. Illingworth (2011). "Evidence That Ice Forms Primarily in Supercooled Liquid Clouds at Temperatures > -27°C". In: *Geophys. Res. Lett.* 38.14. ISSN: 1944-8007. DOI: 10.1029/2011GL048021.

Wex, H., L. Huang, W. Zhang, H. Hung, R. Traversi, S. Becagli, R. J. Sheesley, C. E. Moffett, T. E. Barrett, R. Bossi, H. Skov, A. Hünerbein, J. Lubitz, M. Löffler, O. Linke, M. Hartmann, P. Herenz and F. Stratmann (2019). "Annual Variability of Ice-Nucleating Particle Concentrations at Different Arctic Locations". In: *Atmospheric Chem. Phys.* 19.7, pp. 5293–5311. ISSN: 1680-7324. DOI: 10.5194/acp-19-5293-2019.

Whale, T. F. (2018). "Chapter 2 - Ice Nucleation in Mixed-Phase Clouds". In: *Mixed-Phase Clouds*. Ed. by C. Andronache. Elsevier, pp. 13–41. ISBN: 978-0-12-810549-8. DOI: 10.1016/B978-0-12-810549-8.00002-7.

Winker, D. M., M. A. Vaughan, A. Omar, Y. Hu, K. A. Powell, Z. Liu, W. H. Hunt and S. A. Young (2009). "Overview of the CALIPSO Mission and CALIOP Data Processing Algorithms". In: *J. Atmospheric Ocean. Technol.* 26.11, pp. 2310–2323. ISSN: 0739-0572, 1520-0426. DOI: 10.1175/2009JTECHA1281.1.

Xu, L., S. Fukushima, S. Sobanska, K. Murata, A. Naganuma, L. Liu, Y. Wang, H. Niu, Z. Shi, T. Kojima, D. Zhang and W. Li (2020). "Tracing the Evolution of Morphology and Mixing State of Soot Particles along with the Movement of an Asian Dust Storm". In: *Atmospheric Chem. Phys.* 20.22, pp. 14321–14332. ISSN: 1680-7316. DOI: 10.5194/acp-20-14321-2020.

Yang, X.-Y., J. C. Fyfe and G. M. Flato (2010). "The Role of Poleward Energy Transport in Arctic Temperature Evolution". In: *Geophys. Res. Lett.* 37.14. ISSN: 1944-8007. DOI: 10.1029/2010GL043934.

Zelinka, M. D., T. A. Myers, D. T. McCoy, S. Po-Chedley, P. M. Caldwell, P. Ceppi, S. A. Klein and K. E. Taylor (2020). "Causes of Higher Climate Sensitivity in CMIP6 Models". In: *Geophys. Res. Lett.* 47.1, pp. 1–12. ISSN: 19448007. DOI: 10.1029/2019GL085782.

Zhang, M., S. Xie, X. Liu, W. Lin, K. Zhang, H.-Y. Ma, X. Zheng and Y. Zhang (2020). "Toward Understanding the Simulated Phase Partitioning of Arctic Single-Layer Mixed-Phase Clouds in E3SM". In: *Earth Space Sci.* 7.7, e2020EA001125. ISSN: 2333-5084. DOI: 10.1029/2020EA001125.